



University of
Stavanger

Faculty of Science and Technology

MASTER'S THESIS

Study program/Specialization: Master of Science in Environmental Engineering (Specialization in Offshore Environmental Technology)	Spring semester, 2021 Open access
Writer: Aashish Thapa	 (Writer's signature)
Faculty supervisor: Rune Wiggo Time, Andrianifaliana Herimonja Rabenjafimanantsoa External supervisor(s):	
Thesis title: CO ₂ Absorption and Transportation Modes in Porous Media: Numerical Simulation and Comparison with Laboratory Experiment.	
Credits (ECTS): 30	
Key words: Carbon Capture and Storage (CCS) Pressure Decay Diffusion Convection COMSOL Multiphysics	Pages: 61 + supplement material/others: 14 Stavanger, 15.06.2021 Date/year

THIS PAGE IS INTENTIONALLY LEFT BLANK

Preface

This thesis is submitted in partial fulfillment of the requirements for the degree of Master of Science in Environmental Engineering (Specialization in Offshore Environmental Technology). The thesis is worth 30 credit points. The degree is offered by Department of Chemistry, Bioscience and Environmental Engineering at University of Stavanger. However, the thesis is done with Department of Energy and Petroleum Technology under the supervision of Professor Rune Wiggo Time and Senior Engineer Andrianifaliana Herimonja Rabenjafimanantsoa after getting the permission from my department i.e. Department of Chemistry, Bioscience and Environmental Engineering.

I decided to write my thesis on this topic “CO₂ Absorption and Transportation Modes in Porous Media: Numerical Simulation and Comparison with Laboratory Experiment” due to its applicability in Carbon Sequestration and emerging CCS Technology. Also, the topic is closely related to my specialization which aims towards combining courses in offshore oil and gas exploration, production technologies and environmental management.

Acknowledgments

I want to express my sincere gratitude to Professor Rune Wiggo Time and Senior Engineer Andrianifaliana Herimonja Rabenjafimanantsoa for their guidance and support through entire process of the thesis. I want to acknowledge all the help from Andrianifaliana Herimonja Rabenjafimanantsoa while carrying out the experimental work with a lot of appreciation.

I want to thank Bertil Nistad and Nikolai Ubostad, both working at COMSOL AS, for their advice regarding the COMSOL simulation.

I want to thank Theodor Ivestal at University of Stavanger for all the technical support.

I greatly appreciate the help from my friend Nikolai Westlund while setting up and conducting the experiment.

Abstract

Absorption and mass transfer mechanism of CO₂ in a uniformly distributed porous media was analyzed using simulation as well as experimental results. The study was performed in a closed PVT cell containing pressurized CO₂ gas above a water saturated porous media. Pressure decay curves obtained from the simulation and the experiments were used to calculate early and late time diffusivity in accordance with analytical model. Mixing regime was visualized over time to comprehend the contribution of natural convection in mass transfer process.

Early time diffusion coefficients were two orders of magnitude higher than late time diffusion coefficients in both simulation and experimental results. Density-driven natural convection had a significant impact at early stages giving rise to enhanced mass transfer and hence the disparity in diffusivity. The diffusivity at late stages were close to literature value. Pressure decay observed from large duration simulation results showed that equilibrium was reached at close to theoretical saturation pressure.

Three stages of diffusion were observed in both simulation and experimental pressure decay plots. The first stage indicated rapid pressure decline over a short interval of time. At this stage, upper layer of water saturated porous media at liquid-gas interface establishes an equilibrium with gas column above it. The second stage was convection dominated mass transfer followed by the third stage which was diffusion dominated. Finger propagation observed in the porous media was mainly in downward direction before expanding horizontally.

Nomenclature

Abbreviations

GHGs	Green House Gases
CCS	Carbon Capture and Storage
LBM	Lattice Boltzmann Method
RWPT	Random Walk Particle Tracking
WSPM	Water Saturated Porous Media
PVT	Pressure-Volume-Temperature
BTB	Bromothymol blue
DW	Deionized Water
WBS	Water Based Solution
2D	Two Dimensional
3D	Three Dimensional
tds	Transport of diluted species
dl	Darcy's law
CAD	Computer Aided Design
FEM	Finite Element Method

List of Symbols

J	Molar Flux
D	Diffusion Coefficient
c	concentration
x	displacement

t	time
N_i	Molar flux of species i
D_i	Diffusion coefficient of species i
c_i	Concentration of species i
$N_{i,\text{conv}}$	Convective molar flux of species i
\mathbf{u}	Fluid velocity
Ra	Rayleigh number
κ	Permeability
$\Delta\rho$	Change in density
g	Acceleration due to gravity
d	Characteristic diameter
μ	Dynamic viscosity
P	Pressure
K_H	Henry's constant
C_1	Concentration at liquid-gas interface
z	Length from the bottom of water column
z_0	Length from the bottom of water column to liquid-gas interface
n	Natural number
V	Volume of gas
Z_g	Compressibility factor
R	Universal gas constant
T	Temperature
A	Cross sectional area of the cell

$P(t)$	Pressure at time t
P_{eq}	Saturation pressure or equilibrium pressure
$C_{1,eq(p)}$	Equilibrium liquid-gas interface concentration
h	Height of water column
φ	Average porosity
V_p	Pore volume
V_b	Bulk volume
H	Height of gas column
L	Height of Water Saturated Porous Media
W	Inner radius of the cylindrical cell
rho	Variable Density
rho0	Initial density
c0	Initial CO ₂ concentration in Water Saturated Porous Media
c_s	Initial CO ₂ concentration in gas column
beta	Density increase per mole of CO ₂ absorbed
ε	Porosity
D	Elevation
p	Fluid pressure
∇	Gradient
θ_s	Volume fraction of the fluid
D_L	Diffusion coefficient of gas in the fluid
τD_L	Molecular diffusion rate
q	Water flow rate

P_{atm} Atmospheric pressure

Chemical Symbols

CO_2 Carbon dioxide

NaOH Sodium hydroxide

H_2O Water

Na^+ Sodium ion

OH^- Hydroxide ion

HCO_3^- Bicarbonate ion

CO_3^{2-} Carbonate ion

NaHCO_3 Sodium Bicarbonate

H_2CO_3 Carbonic acid

H^+ Hydrogen ion

Table of Contents

Preface.....	iii
Acknowledgments	iv
Abstract	v
Nomenclature.....	vi
List of Figures	xii
List of Tables	xiv
1 Introduction.....	1
1.1 Objectives	2
1.2 Scope and Limitations.....	2
1.3 Challenges	3
1.4 Organization of the Thesis.....	3
2 Theory.....	4
2.1 Previous Work	4
2.1.1 Transportation in Porous Media.....	5
2.1.2 Pore-Scale Simulation.....	6
2.1.3 Macroscale Modeling in Porous Media	6
2.2 Solubility of CO ₂ in Aqueous Alkaline Solutions	7
2.3 Transport Mechanisms.....	9
2.3.1 Diffusion	9
2.3.2 Convection.....	10
2.3.3 Solubility of Gas into Liquid Phase	10
2.4 Rayleigh Number.....	11
3 Analytical Model.....	12
3.1 Assumptions	12
3.2 Mathematical Formulation.....	13
3.3 Model Validation.....	15
4 Methodology	16
4.1 COMSOL Simulation	16
4.1.1 Defining Space Dimension.....	16

4.1.2	Defining Physics and Study.....	16
4.1.3	Model Builder.....	18
4.1.4	Defining Geometry.....	19
4.1.5	Defining Mesh.....	20
4.1.6	Multiphysics.....	21
4.2	Pressure Decay Experiment.....	22
4.2.1	Experimental Setup.....	22
4.2.2	Experimental Procedure.....	25
5	Results and Discussion.....	26
5.1	Simulation Results and Discussion.....	26
5.1.1	Mixing Regime.....	30
5.2	Experimental Results.....	36
5.2.1	Mixing Regime (Experimental).....	38
6	Conclusion.....	44
	References.....	46
	Appendix A.....	49
	Appendix B.....	58

List of Figures

Figure 2.1: Evolution from molecular to porous-continuum domain (Merrikh & Lage, 2005)	5
Figure 3.1: Diffusion-based model.....	12
Figure 4.1: 2D Axisymmetric icon in COMSOL	16
Figure 4.2: Select Physics window in COMSOL.....	17
Figure 4.3: Select Study window in COMSOL.....	18
Figure 4.4: Model Builder window in COMSOL	19
Figure 4.5: Rectangle 1 and Rectangle 2 Geometries	20
Figure 4.6: Types of elements used for 3D Meshing in COMSOL	20
Figure 4.7: Expression for variable density in COMSOL.....	21
Figure 4.8: CO ₂ absorption system (Hansen, 2020).....	23
Figure 4.9: Porosity and permeability measurement system (Hansen, 2020)	24
Figure 5.1: Concentration vs Time graph from t=0 to t=72 hours.....	26
Figure 5.2: Pressure vs Time graph from t=0 to t=72 hours.	27
Figure 5.3: Concentration vs Time graph from t=0 to t=10000 hours.....	28
Figure 5.4: ln(P(t)-P _{eq}) vs Time graph.....	29
Figure 5.5: Three stages of mass transfer mechanism.	30
Figure 5.6: Mixing regime in WSPM of 45% porosity and 23800 mD permeability from t=0 to t=5 hours.....	32
Figure 5.7: Mixing regime in WSPM of 45% porosity and 23800 mD permeability from t=6 to t=11 hours.....	33
Figure 5.8: Mixing regime in WSPM of 45% porosity and 23800 mD permeability from t=12 to t=17 hours.....	34
Figure 5.9: Mixing regime in WSPM of 45% porosity and 23800 mD permeability from t=18 to t=23 hours.....	35

Figure 5.10: Experimental Pressure Decay Curve	36
Figure 5.11: $\ln(P(t)-P_{eq})$ vs Time graph from the experiment.....	37
Figure 5.12: Three stages of mass transfer mechanism (experimental).....	38
Figure 5.13: Mixing regime from experiment in WSPM of 45% porosity and 23800 mD permeability from $t=0$ min to $t=165$ min (Camera 1: Google Pixel 4a).	40
Figure 5.14: Mixing regime from experiment in WSPM of 45% porosity and 23800 mD permeability from $t=0$ min to $t=105$ min (Camera 2: Nikon D5300).	41
Figure 5.15: Mixing regime from experiment in WSPM of 45% porosity and 23800 mD permeability from $t=120$ min to $t=225$ min (Camera 2: Nikon D5300).	42
Figure 5.16: Mixing regime from experiment in WSPM of 45% porosity and 23800 mD permeability from $t=240$ min to $t=255$ min (Camera 2: Nikon D5300).	43

List of Tables

Table 2.1: Alkaline WBS recipe	7
Table 5.1: Parameters used for P_{eq} calculation.....	28
Table 5.2: Early and late time diffusion coefficients obtained from simulation.....	30
Table 5.3: Early and late time diffusion coefficients obtained from experimental results.	37

1 Introduction

There is a growing concern in the scientific community regarding greenhouse gas emissions and its relationship with world climate change in recent decades. Owing to the ongoing anthropogenic activities, the global ambient CO₂ concentration, which by far has the largest contribution among all greenhouse gases (GHGs), has risen considerably (Posch & Haider, 2013).

Recent studies estimate that more than 60% of global CO₂ emissions are produced by power and industry sectors (Statistics, 2011). In order to achieve the strict goal of not surpassing 2 degrees Kelvin global temperature rise, maintaining an adequate energy supply, scholars throughout the globe are more concerned now than ever (IEA, 2011). General consensus regarding climate change has contributed to the popularity of carbon capture and storage (CCS) technologies which will be significant until renewables can fully replace the present global energy demand (Posch & Haider, 2013).

To tackle the current global warming trend, studies are being carried out for the development of better gas absorption and membrane separation methods aiming to recover and concentrate CO₂ in flue gases. While CO₂ emissions come from numerous sources, such as power plants, industry, domestic heating, traffic, etc., CO₂ mitigation research is mainly focused on power plants and industry to examine the feasibility in these sectors (Mofarahi et al., 2008). Chemical absorption of CO₂ in amine aqueous solutions is regarded one of the most advanced and least costly approaches to be introduced to power plants among the CO₂ recovery alternatives (Erga et al., 1995).

Absorption and fluid flow in porous media is an important area of study in various industries such as oil discovery, filtering, regulation of underground water contamination, drug manufacturing, and electronics. Presence of more than one constituent along with complexity of the interface makes the porous media rather heterogeneous. To reduce the complexity of the transport in porous media, continuum equations are derived by averaging within a small elementary unit of a domain which consider only the net effects of carriers. These effects are defined by continuum parameters like velocity, pressure, and temperature which represent the characteristics in a more feasible manner (Merrikh & Lage, 2005).

Due to the complexity in turbulence as well as the internal morphology of the porous medium, a normal modeling approach would be the application of time averaging (for handling

turbulence) and space averaging (for handling morphology) to microscopic equations (Lage et al., 2002).

Various numerical simulation approaches such as finite element method, semi-analytical method, Lattice Boltzmann Method (LBM) and RWPT (Random Walk Particle Tracking) have been used to solve the steady-state advection-diffusion equation in porous media. In RWPT approach, simulation of advection is done by modelling velocity field obtained from LBM or other methods and simulation of diffusion is done by modelling Brownian motion (Xiao, 2013a).

1.1 Objectives

The main objective of this thesis is to investigate the mechanism of CO₂ absorption in Water saturated porous medium (WSPM). The study is done in a setup where mass transfer of CO₂ between the phases is limited to upper surface of the WSPM exposed to CO₂ as shown figure 4.8. There is a significant utility of the study in sequestration of CO₂ into deep geological formations where pressurized CO₂ gas is pumped into aquifers. To mimic the actual sequestration process, high pressure CO₂ is introduced above the WSPM in a closed PVT cell and pressure decay is observed over time. Pressure decay is observed both through experiment and simulation created using COMSOL Multiphysics - Version 5.4 software. As dissolution progresses, it is eminent that density at upper part of the WSPM becomes higher than underlying layers due to absorbed CO₂. Thus created density difference is likely to create a density-driven natural convection in the WSPM. It is expected that this density-driven convection has a significant impact on effective diffusion coefficient at earlier stages.

1.2 Scope and Limitations

Scope of this thesis is confined to the study of CO₂ absorption and transport mechanisms in Water Saturated Porous Media (WSPM) using numerical simulation and experimental work. Pressure decay data and mixing regime are used to identify the role of density difference in the onset of natural convection. Due to its negligible contribution to the transport mechanism, chemical reactions between CO₂ and water is considered insignificant. Also, if similar method is to be applied to imitate marine environment, the effects of salinity should be considered.

1.3 Challenges

Leakage was the main challenge during experimental work because of high pressure CO₂ gas. Many failed experiments had to be conducted before achieving desired results. Also, closing the valves at exact timing was tricky. Due to time limitations, experiment couldn't be repeated over longer time interval. Visibility of the mixing regime was compromised due to the presence of porous medium because the blue solution could only occupy the interparticle space between the glass beads. Also, built-in functions in COMSOL had limited flexibility which made it challenging to tailor the simulation as desired.

1.4 Organization of the Thesis

Chapter 2 contains theory of previous works done in the field of absorption in porous media. It also sheds light to different mass transport mechanisms involved in the study. Chapter 3 contains analytical model and related derivations. Chapter 4 contains methodology for both simulation and pressure decay experiment conducted. Chapter 5 contains results and discussion from the simulation and the experiment and comparison between them. Chapter 6 contains the takeaways and conclusion from the study.

2 Theory

2.1 Previous Work

Gmelin (1968) demonstrated that concentration gradient as well as density gradient develops due to the dissolution of CO_2 as it comes in contact with water surface. In other words, the water at upper layers becomes denser compared to lower layers. Thus formed density gradient instigates natural convection. This ultimately leads to higher mass transfer rate of CO_2 into the water and hence a higher flux at water- CO_2 interface. With time, density gradient decreases as the system becomes more homogeneous in terms of concentration. After a certain point, natural convection becomes less significant and diffusion becomes the dominant mass transfer mechanism (R. Farajzadeh et al., 2007).

The effect of natural convection in mass transfer mechanism of CO_2 were proposed by Lindeberg & Wessel-Berg (1997), Yang & Gu (2006). Although the work of Lindeberg & Wessel-Berg (1997) lacked any quantification, their study strongly suggested the presence of natural convection due to density increase when CO_2 was injected into saline aquifers. Similarly, Yang & Gu (2006) conducted mass transfer experiments under high temperature and pressure and used modified diffusion equations to calculate effective diffusion coefficients. Their results showed that effective diffusion coefficients were two orders of magnitude higher than the literature value of molecular diffusivity of CO_2 in water. Although each experiment was run for relatively short duration, it was quite evident that natural convection due to density gradient had significant impact on the mass transfer of CO_2 at initial stages.

Farajzadeh (2009) conducted mass transfer experiments for longer duration on both water and hydrocarbon-based solutions. He also noticed that effective diffusion coefficients¹ calculated at early stages were two orders of magnitude higher than the molecular diffusivity of CO_2 in water. However, the calculated long-time effective diffusion coefficients were quite comparable to literature values.

Mojtaba et al. (2014) investigated the role of density-driven convection in CO_2 dissolution in saline aquifers. The effect of natural convection in the dissolution process seemed to fade away

¹ The term “effective diffusion coefficient” is used to acknowledge varying diffusivity values at different stages of the mass transport process, meaning diffusion coefficient in effect at a certain stage.

with time until it reached zero at later stages. This was because the driving force i.e. density gradient decreased over time.

Although numerous experimental techniques have been applied over time, no universal method has been developed to calculate diffusion coefficients in fluids yet. This is because the experiments are usually time consuming and expensive because they demand detailed compositional analysis (Moulu, 1989).

2.1.1 Transportation in Porous Media

Figure 2.1 shows the evolution of domains from molecular resolution level to continuum resolution level and eventually to porous-continuum level all of which demand an averaging process. However, there are shortcomings in its applicability because the scales are represented by inequalities and hence, the validity of the continuum equations to model the transport process is difficult to assess (Merrikh & Lage, 2005).

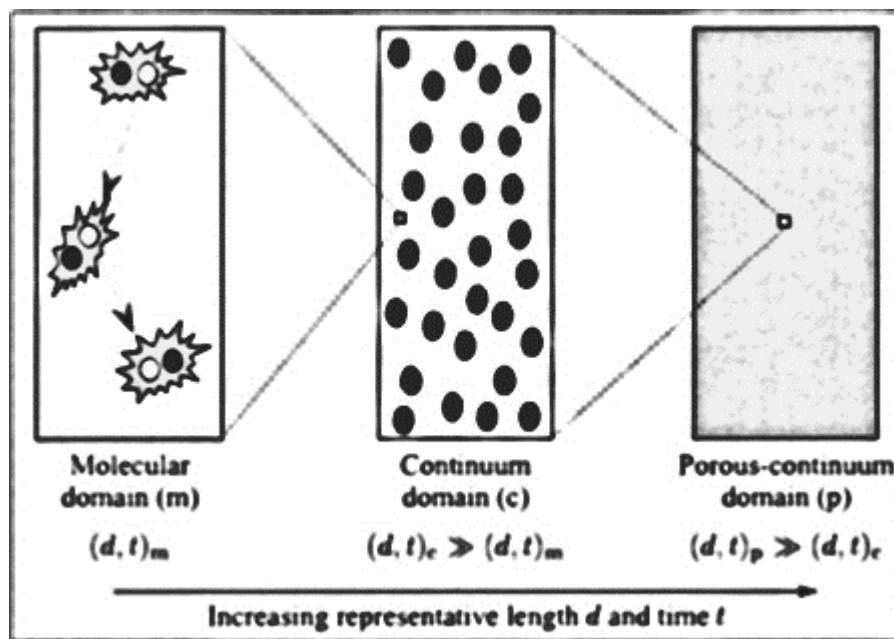


Figure 2.1: Evolution from molecular to porous-continuum domain (Merrikh & Lage, 2005)

Although porous media is dealt with macroscopic level of understanding for ease in practical applications, modeling however initiates in the pore-scale as a basis for eventually upscaling to larger scales. The exploration is no longer limited to macroscopic parameters such as permeability, porosity and so on but also the microstructures and pore scale transport behavior such as phase change, fluid-structure interaction, activated processes and so forth (Peng & Wu, 2005).

2.1.2 Pore-Scale Simulation

With the emergence of sophisticated algorithms along with parallel computation, pore-scale direct numerical simulations have become important methods for averaging microscopic mechanisms and uncovering average macroscopic behaviors. Numerical simulation to solve control equations such as Navier-Stokes equation and Advection-Diffusion equation for pore-scale phenomena is fundamental to the understanding of transport mechanisms. These pore-scale simulations provide a basis for modeling complex fluid dynamics as well as complex geometry of pores (Xiao, 2013).

The main categories of simulation approaches in fluid dynamics include continuum approaches, pseudo-particle approaches and molecular dynamics (Raabe, 2004). Molecular dynamics integrates Newton's equations of motion for molecules based on intermolecular potentials. A pseudo particle, which actually represents a mesoscopic cluster of molecules, is best described by Lattice Boltzmann method which sees the flow as a collective dynamics of pseudo particles. As we go higher to the continuum approach, Navier-Stoke's equation is used to formulate mass and momentum conservation through differential methods (Xiao, 2013b).

2.1.3 Macroscale Modeling in Porous Media

Modeling flow in heterogeneous media, which often includes multiple scales such as different length and time scales controlling the dynamics of the flow, is a constant challenge not only in terms of predictability of the model but also its efficiency during computation. Macroscopic models, which are averaged representations of micro-scale processes have proven to be more efficient for computation compared to microscale models. Consequently, the macro-scale approach has been recognized as more viable in decision making process for practitioners who are usually concerned with predictions and optimization of the system performance as a whole (Battiato et al., 2019).

According to upscaling tools proposed by Cushman (1990) and reviewed by Cushman et al. (2002), complementary hierarchies can be classified into two sets: 1. Structural-functional, and 2. Discrete vs continuous. Structural hierarchy in a porous medium can be described as a hierarchy decomposable into successively nested, interacting subunits whereas, functional hierarchy in a porous medium is concerned with hierarchical transport processes within the medium. Similarly, the main difference between discrete and continuous hierarchical systems is that, in discrete system, constitutive laws are local whereas in continuous system, constitutive laws are non-local (Cushman et al., 2002).

Despite considerable progress in recent decades in the field of flow and transport in porous media, there is a challenge in understanding the system response at macroscale on the basis of pore-scale processes, largely considering the disparity in scales between those models (Anna et al., 2014). For instance, in reactive multiphase systems, where the distribution between the phases is complex along with unstable interfaces between them, the upscaling methods traditionally used to construct effective models do not seem to be very convincing (Jiménez-Martínez et al., 2015).

2.2 Solubility of CO₂ in Aqueous Alkaline Solutions

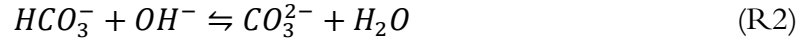
The composition of water-based solution (WBS) used in the experiment for this thesis is presented in table 2.1. Addition of Sodium hydroxide (NaOH) makes the aqueous solution alkaline (pH = 11). This is done because the dissolution of CO₂ makes the solution acidic during the experiment and hence makes the visualization of mixing regime possible. So, before any absorption has occurred, the solution will appear bluish in alkaline environment which is the color of Bromothymol blue (BTB) indicator. When absorption of CO₂ in the aqueous solution occurs over time, the solution will start turning yellowish. Through this colour change in the WBS, visualization of mixing regime and hence the analysis of transport mechanisms in the Water Saturated Porous Media (WSPM) becomes easier.

Table 2.1: Alkaline WBS recipe

Compound	Amount
Deionized water (DW)	5L
5% Sodium hydroxide (NaOH)	4 ml
Bromothymol blue (BTB)	50ml

Before the introduction of CO₂, the NaOH has ionized into Na⁺ and OH⁻ ions. The high pH is due to the presence of OH⁻ ions.

When CO₂ is absorbed into the aqueous alkaline solution CO₂(aq) will be instantly consumed. The chemiabsorption of CO₂ in aqueous sodium hydroxide follows two major steps of reaction mechanism:

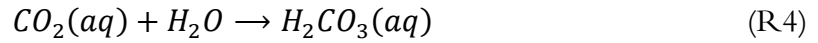


Both reactions are reversible and have high effect on pH changes. As CO₂ is getting absorbed, the OH⁻ concentration will decrease and CO₃²⁻ concentration will increase. The increase in CO₃²⁻ concentration will force a backward reaction of R2 and accelerate the forward reaction of R1. When the reactions reach equilibrium, the overall reaction of CO₂ and NaOH is given by R3 (Adnan et al., 2020).

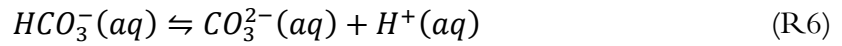
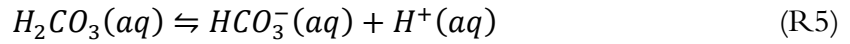


However, the total amount of CO₂ absorbed by NaOH in the system can be neglected because the concentration of NaOH in the prepared WBS is substantially small. Addition of NaOH in the WBS is done solely for observing visual effects with BTB.

The reaction of CO₂ with water to form carbonic acid is written as:



Thus formed H₂CO₃ can lose one or both hydrogen ions:



Due to the released H⁺ ions, pH drops. However, it should be noted that the reaction is reversible. At higher pH, backward reaction of R2 is expected i.e. CO₃²⁻ will take H⁺ ions to form more HCO₃⁻. But, in the system where CO₂ is adequately supplied, forward reactions of R5 and R6 are expected to occur increasing the H₂CO₃ concentration and hence decreasing the pH until an equilibrium is established (Adnan et al., 2020).

CO₂(g) is quite soluble in water. It is estimated that more than 99% of the dissolved CO₂ exists as CO₂(aq) and less than 1% exists as H₂CO₃ which partly dissociates to give H⁺, HCO₃⁻ and CO₃²⁻ ions. (Knoche, 1980). Hence, the chemical reactions involving the formation of H₂CO₃ have not been considered in simulation in this thesis.

2.3 Transport Mechanisms

2.3.1 Diffusion

Diffusion can be defined as a spontaneous process involving random motion of particles as a result of concentration gradient established in a space. For a system where concentration changes with displacement, molar flux due to diffusion is proportional to concentration gradient and is given by Fick's first law:

$$J = -D \frac{\partial c}{\partial x} \quad (2.1)$$

Where, J is the flux ($\text{mol m}^{-2} \text{s}^{-1}$) i.e. the number of moles of particles passing through a unit area per unit time. D is the diffusion coefficient ($\text{m}^2 \text{s}^{-1}$), c is the concentration (mol m^{-3}), and x is the displacement.

Fick's law is applicable to steady state systems where the net change in incoming flux and outgoing flux is zero. For unsteady systems with variable solutions, Fick's second law can be applied and is written as:

$$\frac{\partial c}{\partial t} = D \frac{\partial^2 c}{\partial x^2} \quad (2.2)$$

Where, $\frac{\partial c}{\partial t}$ is the rate of change of concentration in a certain area and $\frac{\partial^2 c}{\partial x^2}$ is the changes that the change in concentration can incur. For a system where concentration does not change, $\frac{\partial^2 c}{\partial x^2}$ becomes zero (*Diffusion*, 2021).

In modern mathematical form, Fick's first law can be written as:

$$N_i = -D_i \nabla c_i \quad (2.3)$$

Where, N_i is the molar flux ($\text{mol m}^{-2} \text{s}^{-1}$), D_i is the diffusion coefficient ($\text{m}^2 \text{s}^{-1}$), and c_i is the concentration (mol m^{-3}) for species i .

The continuity equation for mass can be written as:

$$\frac{\partial c_i}{\partial t} + \nabla \cdot N_i = 0 \quad (2.4)$$

Substituting N_i from Eq. 2.3 to Eq. 2.4, we get Fick's second law:

$$\frac{\partial c_i}{\partial t} = D_i \nabla^2 c_i \quad (2.5)$$

Eq. 2.4 assumes that D_i is a constant and is true for diffusion of chemical species in dilute solutions (*Diffusion Equation: Fick's Laws of Diffusion*, n.d.)².

2.3.2 Convection

Convection can be defined as mass transport of species due to average velocity field of the fluid. When convection in a bulk fluid contributes to the flux of species i , we can write:

$$N_{i,conv} = c_i \mathbf{u} \quad (2.6)$$

Where, $N_{i,conv}$ is the molar flux ($\text{mol m}^{-2} \text{s}^{-1}$) and c_i is the concentration (mol m^{-3}) for species i . \mathbf{u} is the fluid velocity (m s^{-1}).

Substituting $N_{i,conv}$ into the mass continuity equation gives:

$$\left(\frac{\partial c_i}{\partial t} \right)_{conv} = -\nabla \cdot N_{i,conv} = -c_i \nabla \cdot \mathbf{u} - \mathbf{u} \cdot \nabla c_i \quad (2.7)$$

For an incompressible fluid, the first term becomes zero considering the conservation of mass of the fluid as a whole. Hence, Eq. 2.7 reduces to:

$$\left(\frac{\partial c_i}{\partial t} \right)_{conv} = -\mathbf{u} \cdot \nabla c_i \quad (2.8)$$

This is a time dependent, first-order partial differential form of the convection equation. The concentration at a point is subject to change only in the presence of concentration gradient (*What Is Convection?*, n.d.)³.

2.3.3 Solubility of Gas into Liquid Phase

Henry's law provides a quantitative approach to the solubility of a gas in a solvent in relation to the pressure. The law states that at constant temperature, the concentration of gas in solution is proportional to the partial pressure of the gas above the solution.

²

³ These in-text citations contain no author names or publication dates because they are self-generated references (by Zotero software) from COMSOL Multiphysics® official website. Respective links are given in the References.

$$c \propto P \quad (2.9)$$

Where, c (mol m^{-3}) is the concentration of gas in the solution and P (Pa) is the partial pressure in the gas phase.

Introducing the constant of proportionality, the equation can be written as:

$$P = K_H c \quad (2.10)$$

Where, K_H is called Henry's Law constant ($\text{m}^3 \text{ Pa mol}^{-1}$) unique to a specific solute-solvent at a specific temperature.

To determine the molar solubility of gas, the equation can be rearranged as:

$$c = \frac{1}{K_H} \times P \quad (2.11)$$

Where, $\frac{1}{K_H}$ is the inverse of Henry's law constant ($\text{mol m}^{-3} \text{ Pa}^{-1}$).

2.4 Rayleigh Number

An important parameter which can predicts the onset of natural convection is Rayleigh number. The Rayleigh number depends on fluid properties and geometry of the system (Farajzadeh, 2009).

For absorption of gas phase into a liquid saturated porous media, Khosrokhavar et al. (2014) defined Rayleigh number as a function of both fluid and porous media properties:

$$Ra = \frac{\kappa \Delta \rho g d}{\varphi \mu D} \quad (2.12)$$

Where, κ is permeability and φ is porosity of the porous media, $\Delta \rho$ is change in density, g is acceleration due to gravity, d is characteristic diameter of the porous media, μ is dynamic viscosity of the fluid, and D is diffusivity of the gas in the fluid.

Lapwood (1948) determined that the onset of natural convection occurs at Rayleigh number greater than $4\pi^2 \approx 40$.

3 Analytical Model

The physical system consists of a cylindrical cell of constant volume. Porous media is filled to a certain height inside the cell and rest of the volume is to be filled with pressurized CO_2 gas. After attaining required pressure, the cell is sealed and isolated from surroundings. Then, pressure decay due to dissolution of $\text{CO}_2(\text{g})$ into $\text{CO}_2(\text{aq})$ is monitored over time. The system is assumed to be under isothermal condition throughout the process. Following mathematical formulation in this chapter will be primarily based on Zhang et al. (2000). The derivation for the most part is done for CO_2 -water system. When porous media is used instead of water, porosity is inserted in the formulation. Boundary conditions applicable to diffusion-based model of concern are presented in figure 3.1.

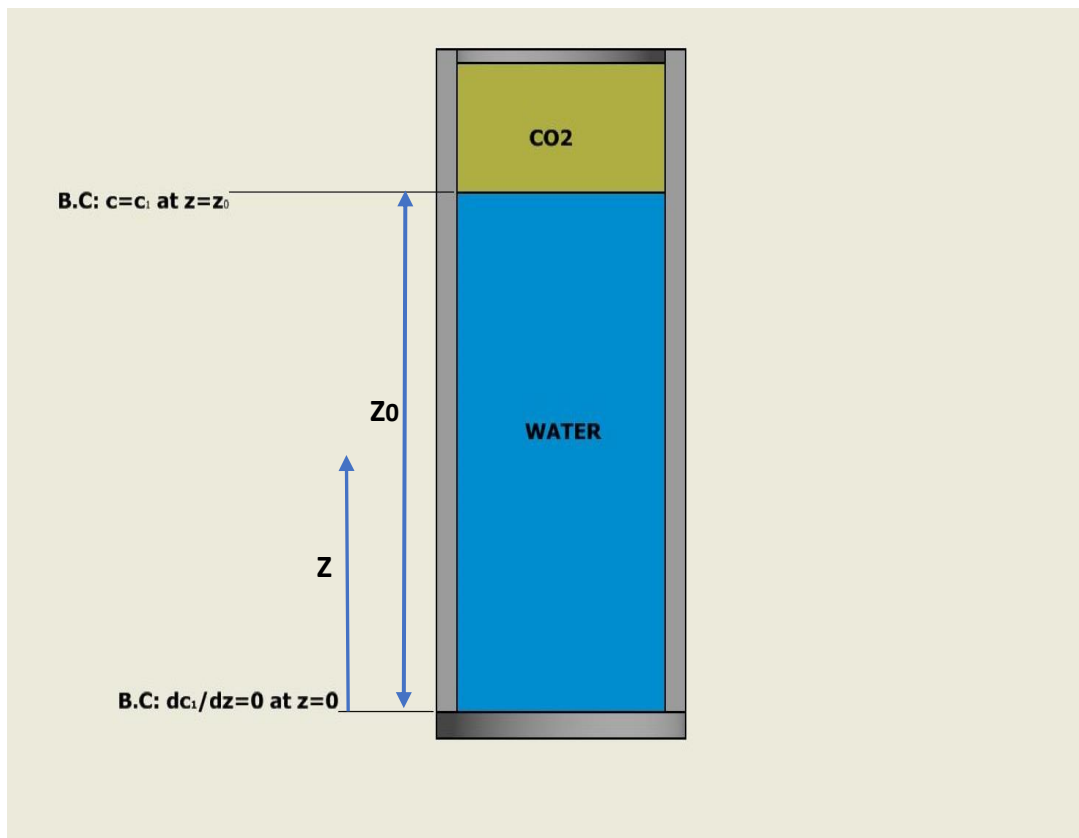


Figure 3.1: Diffusion-based model

3.1 Assumptions

The mathematical model used to determine diffusion coefficient is same as Zhang model due to its simplicity and accuracy. The basic assumption's in Zhang's model are as follows:

- i. Only one-way diffusion i.e. from gas to liquid phase is considered. Water is assumed to be non-volatile.
- ii. Volume change of water column due to dissolution of CO₂ is considered negligible.
- iii. The concentration at liquid-gas interface is same as the equilibrium concentration.
- iv. The gas phase used in the experiment is in pure state.

3.2 Mathematical Formulation

Considering the model as one-dimensional unsteady diffusion, Fick's second law can be used to formulate the change in concentration with respect to time. Assuming constant diffusivity at each saturation interval, a linear homogeneous PDE can be written as:

$$\frac{\partial C_1}{\partial t} = \frac{\partial^2 C_1}{\partial z^2} \quad (3.1)$$

The initial and boundary conditions as shown in figure 3.1 are:

$$\begin{aligned} z < z < z_0, t = 0, C_1 = 0, \\ z = 0, \text{ at all } t, \frac{\partial C_1}{\partial z} = 0, \\ z = z_0, t > 0, C_1 = C_{1,eq(p)} \end{aligned} \quad (3.2)$$

Here, $C_{1,eq(p)}$ is the equilibrium liquid-gas interface concentration dependent on pressure and temperature. Initially, concentration of CO₂ in water phase is considered zero. Since isothermal condition is assumed, the equilibrium liquid-gas interface concentration depends only on the pressure. Solving equation 3.1 with above boundary and initial conditions gives:

$$\begin{aligned} C_1 = C_{1,eq(p)} - \frac{4C_{1,eq(p)}}{\pi} \sum_{n=0}^{\infty} \frac{(-1)^n}{2n+1} \times \cos \frac{(2n+1)\pi z}{2z_0} \\ \times \exp \left(-\frac{(2n+1)^2 \pi^2 D}{4z_0^2} t \right) \end{aligned} \quad (3.3)$$

Mass balance can be used to relate the pressure to diffusion. For mass balance relation, it can be said that the number of moles of CO₂ removed from gas phase is equal to the number of moles transferred across the liquid-gas interface.

$$\frac{V}{Z_g RT} \frac{dP(t)}{dt} = -DA \left(\frac{dC_1}{dz} \right)_{z=z_0} \quad (3.4)$$

Since volume of gas and cross sectional area of the cell are constant, Equation 3.4 can be written as:

$$\frac{dP(t)}{dt} = \frac{Z_g RT}{h} D \left(\frac{dC_1}{dz} \right)_{z=z_0} \quad (3.5)$$

Constant Z_g is the compressibility factor. Integrating from time t to infinity gives:

$$\int_{P(t)}^{P_{eq}} dP(t) = -BD \int_t^{\infty} \left(\frac{dC_1}{dz} \right)_{z=z_0} dt \quad (3.6)$$

Where,

$$B = \frac{Z_g RT}{h} = \text{constant} \quad (3.7)$$

If we differentiate Eq. 3.3 with respect to z (at $z = z_0$),

$$\left(\frac{dC_1}{dz} \right)_{z=z_0} = \frac{2C_{1,eq(p)}}{z_0} \times \sum_{n=0}^{\infty} \exp\left(-\frac{(2n+1)^2 \pi^2 D}{4z_0^2} t\right) \quad (3.8)$$

Substituting $\left(\frac{dC_1}{dz} \right)_{z=z_0}$ from Eq. 3.8 to Eq. 3.6, we can write:

$$P(t) - P_{eq} = \frac{8Bz_0 C_{eq(p)}}{\pi^2} \times \sum_{n=0}^{\infty} \frac{1}{(2n+1)^2} \times \exp\left(-\frac{(2n+1)^2 \pi^2 D}{4z_0^2} t\right) \quad (3.9)$$

Convergence occurs at large values of t . Hence, Eq. 3.9 approximately becomes:

$$P(t) - P_{eq} = \frac{8Bz_0 C_{eq(p)}}{\pi^2} \times \exp\left(-\frac{\pi^2 D}{4z_0^2} t\right) \quad (3.10)$$

Eq. 3.10 can also be written as:

$$\ln(P(t) - P_{eq}) = \ln\left(\frac{8Bz_0 C_{eq(p)}}{\pi^2}\right) + \left(-\frac{\pi^2 D}{4z_0^2} t\right) \quad (3.11)$$

Diffusion coefficient (D) can be obtained from the slope by plotting the experimental data in accordance with Eq. 3.11 (Moghaddam et al., 2012).

3.3 Model Validation

Expression for theoretical saturation pressure i.e. P_{eq} is derived using Henry's law, real gas law, and mass conservation law. P_{eq} can be calculated using Eq. 3.12.

$$P_{eq} = \frac{P_0 K_H h}{K_H h + Z_g R T L} \quad (3.12)$$

For porous media, liquid space is related to average porosity of the media. Average porosity, $\varphi = V_p/V_b$, is simply the ratio of pore volume to bulk volume of the porous media. The theoretical saturation pressure can therefore be written as:

$$P_{eq(porous)} = \frac{P_0 K_H h}{K_H h + Z_g R T L \varphi} \quad (3.13)$$

To validate the model, value of the calculated $P_{eq(porous)}$ can be compared with the experimental data.

4 Methodology

4.1 COMSOL Simulation

Simulation was created using COMSOL Multiphysics® version 5.4 software. Purpose of the simulation was to observe pressure decay over time and compare it with experimental results. Also, the objective was to observe the effect of density increase on density-driven natural convection through the simulation.

4.1.1 Defining Space Dimension

The model was built under 2D axisymmetric space dimension which we can choose while creating a new file in COMSOL Multiphysics application. The icon 2D axisymmetric appears as shown in figure 4.1. In 2D axisymmetric dimension, only half of the cylindrical cell is defined. So, height and radius are input parameters used to define a plane assumed to rotate symmetrically around a central axis resembling a cylindrical geometry.

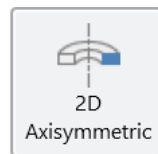


Figure 4.1: 2D Axisymmetric icon in COMSOL

4.1.2 Defining Physics and Study

After defining space dimension, next step is to select the type of physics involved in simulation. Under “Select Physics” window, Transport of Diluted Species (tds) and Darcy’s Law (dl) were selected. The “Select Physics” menu appears as shown in figure 4.2. Any number of physics can be selected as required by the model and integrated in the multiphysics interface.

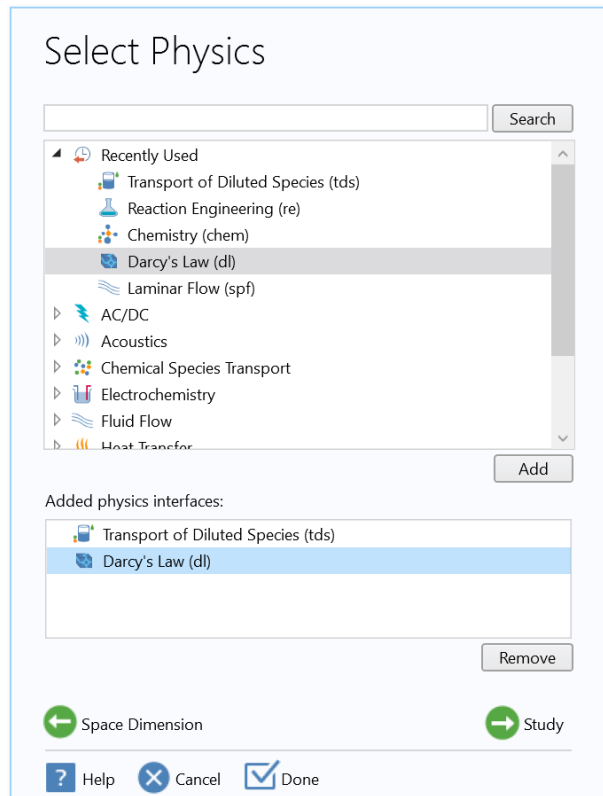


Figure 4.2: Select Physics window in COMSOL

The tds interface in COMSOL can be used to compute concentration field of a dilute solute in a solvent. Diffusion by Fick’s law as well as convection, when coupled with fluid flow, can be used to compute the transport of species dissolved in a fluid. Similarly the dl interface simulates fluid flow in porous media with low-velocity flows driven by pressure gradient and greatly influenced by friction in the porous space (*COMSOL Multiphysics®*, 2018).

After defining the physics, next step was to select the type of study. Under “Select Study” window, “Time Dependent” study was chosen. Since field variables change over time, Time Dependent Study was chosen so that concentration profile could be obtained at different time intervals. Figure 4.3 shows the “Select Study” window.

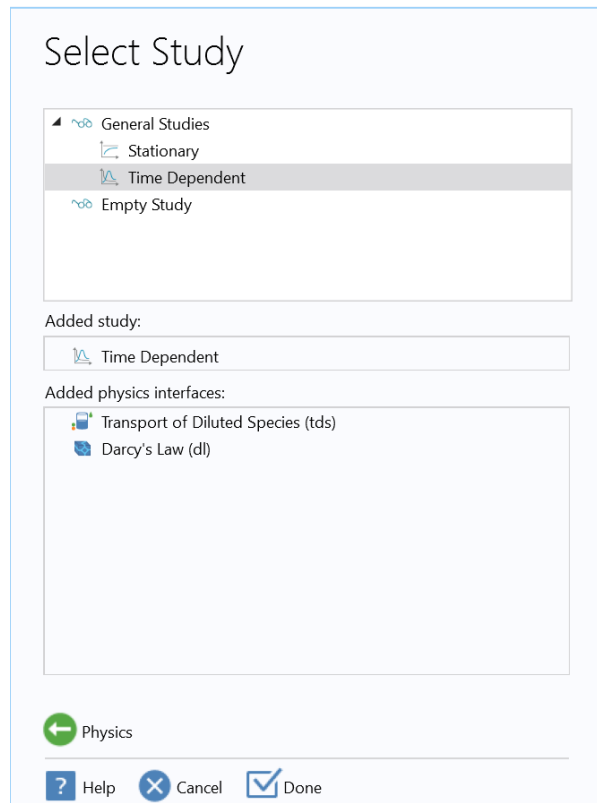


Figure 4.3: Select Study window in COMSOL

4.1.3 Model Builder

Figure 4.4 shows the Model Builder window as it appears in COMSOL Multiphysics® version 4.4. The Model Builder acts as a checklist/guideline for building the model. Usually top to bottom approach is followed. The Global Parameters to be used in the model are defined first. All Definitions, Geometries, Material properties, Multiphysics, Mesh selections are entered sequentially. The overall algorithm of the model is presented in Appendix A.

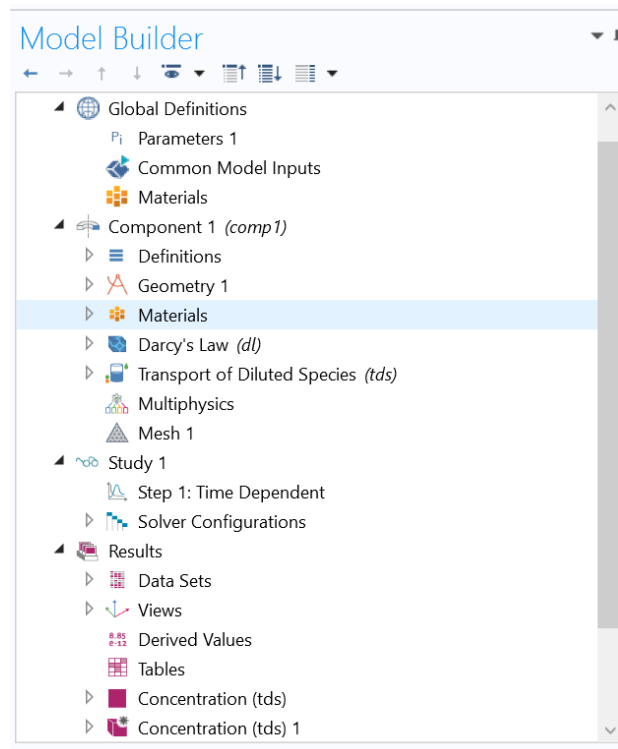


Figure 4.4: Model Builder window in COMSOL

4.1.4 Defining Geometry

Two separate geometries were defined for CO₂ gas column (Rectangle 1) and Porous Media column (Rectangle 2) as shown in figure 4.5. H and L represent CO₂ gas column and Water Saturated Porous Media (WSPM) heights inside the cylindrical cell. W represents inner radius of the cylinder and is same for both CO₂ gas column and WSPM.

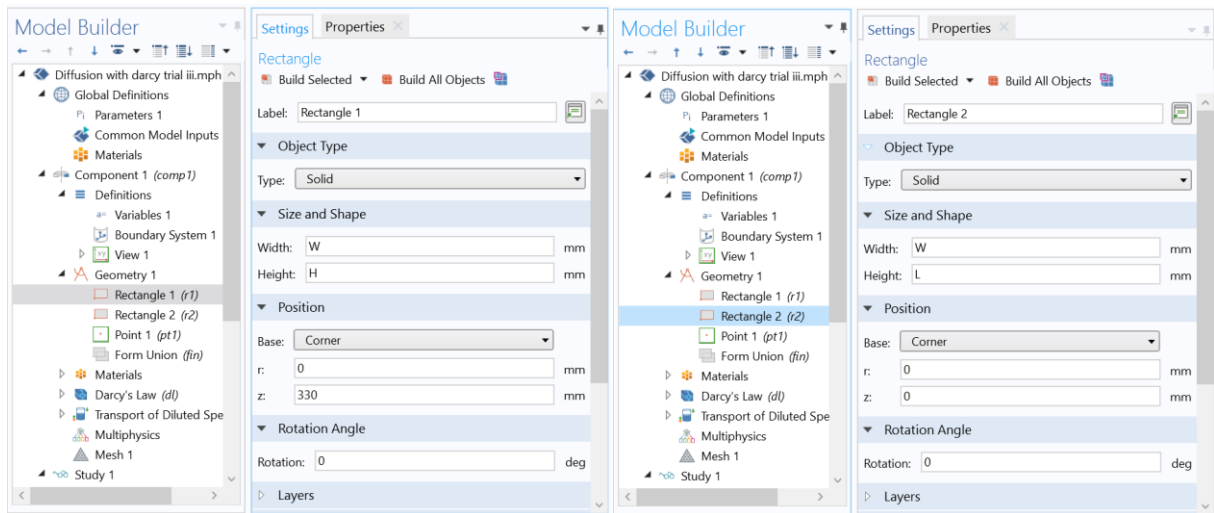


Figure 4.5: Rectangle 1 and Rectangle 2 Geometries

4.1.5 Defining Mesh

Finite Element Method (FEM) is used by COMSOL for dividing the CAD geometry into smaller elements to create a mesh which represents the solution field to the physics involved.

For geometric discretization in 3D Mesh, four different types of elements can be used as shown in figure 4.6: tetrahedra (tets), hexahedra (bricks), triangular prismatic (prisms), and pyramid elements. The grey circles denote the nodes of the elements. The four elements are used by COMSOL in any combination to create mesh as required by the model.

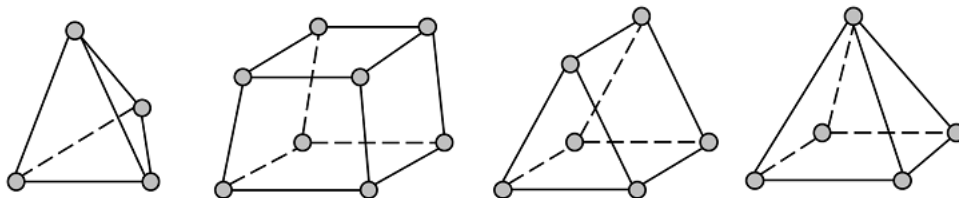


Figure 4.6: Types of elements used for 3D Meshing in COMSOL

Since the model in this thesis is defined under 2D axisymmetric dimension, 2D elements i.e. triangles and quadrilaterals are used by COMSOL. We can define the mesh to be fine or coarse as per the requirement. Although it is always possible to find a solution with coarser mesh, finer mesh is recommended for accuracy. Also, even within a model, elements at the boundaries seem to be finer distributed compared to rest of the area (Walter, 2013).

4.1.6 Multiphysics

As we can see from the model builder window, two physics were chosen for building the model: Transport of Diluted Species (tds) and Darcy's Law (dl). The dependent variables for tds interface and dl interface are concentration and pressure respectively.

Since the density in our model increases with CO₂(aq) concentration, concentration dependent density was defined as shown in figure 4.7.

Name	Expression	Unit	Description
rho	rho0+beta*c*(c>0)	kg/m ³	Water density

Figure 4.7: Expression for variable density in COMSOL

$$\rho = \rho_0 + \beta * c * (c > 0) \quad (4.1)$$

Here, ρ is the variable density, ρ_0 is the initial density before any absorption has occurred, β is the density increase per mole of CO₂ absorbed, and c is the concentration of CO₂.

The fluid flow in WSPM can be described by Darcy's law:

$$\frac{\partial \varepsilon \rho}{\partial t} + \nabla \cdot \rho \mathbf{u} = 0 \quad (4.2)$$

$$\mathbf{u} = -\frac{\kappa}{\mu} (\nabla p + \rho \mathbf{g}) \quad (4.3)$$

Where, ρ is the water density (kg/m³), t is the time (s), \mathbf{u} is the Darcy velocity vector dependent on permeability κ (m²), ε is the porosity, μ is dynamic viscosity of the fluid (Pa.s), p is the fluid pressure (Pa), and \mathbf{g} is the acceleration due to gravity (m/s²). The gradient ∇ of the elevation D (m) denotes the direction of vertical coordinate y .

Change in concentration field of dissolved CO₂ was modelled by Transport of Diluted Species in Porous Media interface. The velocity \mathbf{u} in the governing equation comes from dl interface.

$$\frac{\partial \theta_s c}{\partial t} + \mathbf{u} \cdot \nabla c - \nabla \cdot \theta_s \tau D_L \nabla c = 0 \quad (4.4)$$

Where, θ_s is volume fraction of the fluid i.e. porosity, τD_L is molecular diffusion rate (m^2/s), c is the CO_2 concentration (mol/m^3), \mathbf{u} is Darcy velocity (m/s), and D_L is diffusion coefficient of gas in the fluid (*Models.Ssf.Buoyancy_darcy_elder.Pdf*, n.d.)⁴.

4.2 Pressure Decay Experiment

Riazi (1996) suggested pressure decay method to determine diffusion coefficients of gases in liquids. Inside a PVT cell, pressurized gas is placed in direct contact with underlying liquid. As the gas starts dissolving into the liquid, pressure starts going down with time. The process continues until an equilibrium is established and the liquid becomes saturated with the gas. Riazi's model has been often used for studying diffusion mechanisms due to its simplicity and wide range of applicability.

4.2.1 Experimental Setup

Figure 4.8 shows the basic experimental layout. A cylindrical cell of 1380 ml volume and 66 mm internal diameter was used to contain water saturated porous media (WSPM) and CO_2 gas of 99.99% purity. Glass beads of 1mm diameter saturated by WBS (prepared as shown in table 2.1) was used as the WSPM. Two cameras (Camera 1: Google Pixel 4a and Camera 2: Nikon D5300) were placed at 90 degrees angle with each other to take photographs and videos to capture flow dynamics of absorbed CO_2 into the porous medium. The cell was kept inside a rectangular container to prevent cameras' views from getting compromised due to convex cylinder geometry. A ruler was placed inside the container to monitor the water level and CO_2 plume as it got absorbed into the porous medium. A three-way valve placed on top of the cell, as shown in figure 4.8, controlled CO_2 influx from the gas container and into the pressure sensor. To seal the top of the cell, Silicon Grease (SGM494) was applied on the tube threads. It was difficult to measure temperature inside the cell continuously. So, as one of the limitations, isothermal condition was assumed throughout the period of the experiment. Pressure was monitored continuously using a standard PASCO Absolute Pressure Sensor (Model: PASPort PS-2146). CO_2 gas could be pumped from the top and water could be drained from the bottom as per the requirement.

⁴ This in-text citation contains no author name or publication date because it is a self-generated reference (by Zotero software) from COMSOL Multiphysics® official website, the link to which is given in the References.

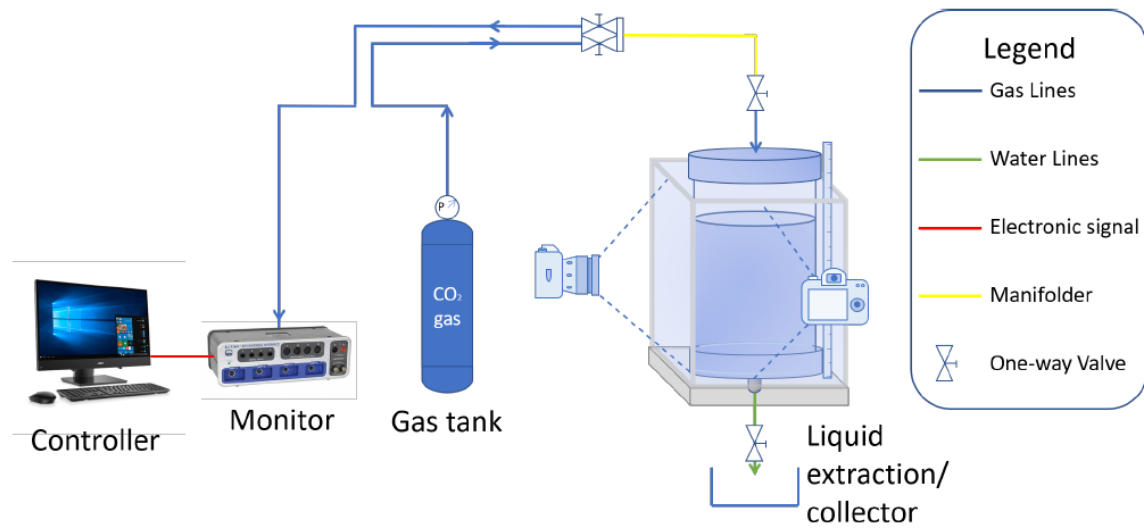


Figure 4.8: CO₂ absorption system (Hansen, 2020)

4.2.1.1 Porosity and Permeability of Porous Media

The porosity and permeability data for the porous media containing glass beads of average diameter 1mm was taken from the experiments done at University of Stavanger by Hansen (2020). The experimental setup used for porosity and permeability measurements is shown in figure 4.9.

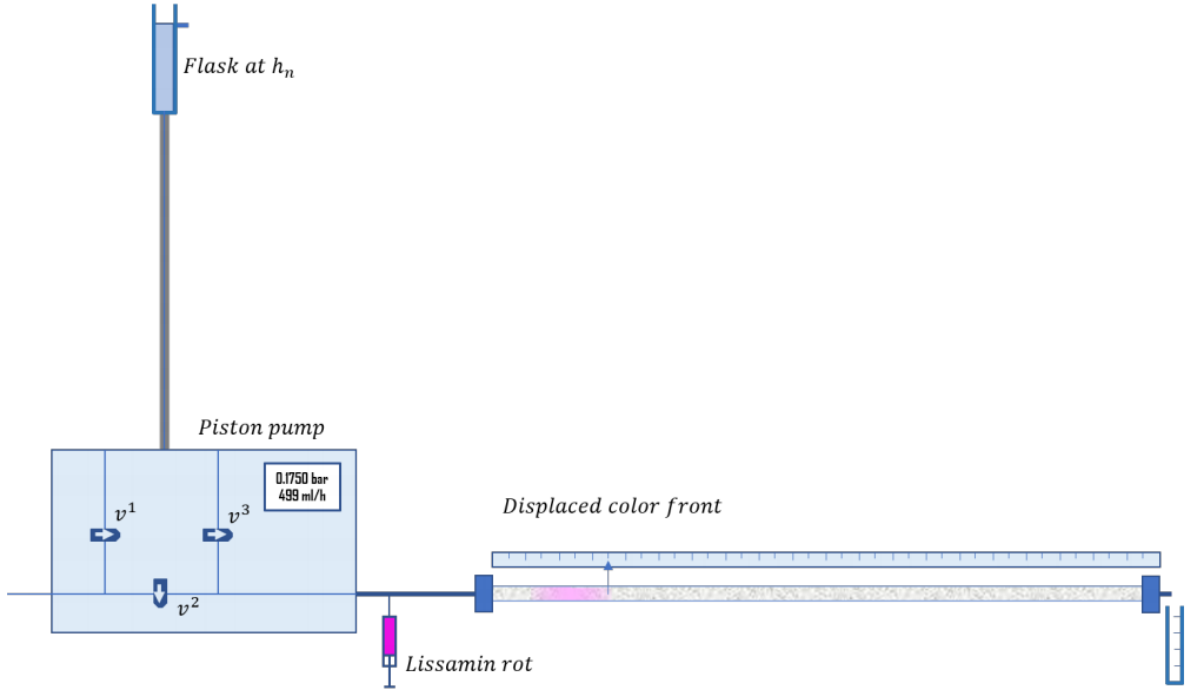


Figure 4.9: Porosity and permeability measurement system (Hansen, 2020)

At the beginning $v1$, $v2$ and $v3$ valves had been closed. For porosity measurement, glass beads in a glass tube were made water saturated by pumping water at a rate q for an hour. Porosity was measured by injecting a color, i.e. lissamin rot, through the glass tube. The displacement of the color front was plotted against time to obtain a straight line of best fit. Gradient dx/dt was put in the following equation to obtain porosity:

$$q = \varphi A \frac{dx}{dt} \quad (4.5)$$

Where, φ is the porosity and A is the cross section area of the glass tube.

For permeability measurement, $v2$ was kept closed. A flask kept at height h_n contained a constant volume of water at all times to maintain a constant hydrostatic pressure to the glass tube. Valve $v1$ was used for pumping in and taking out excess water from the flask. To start the experiment $v3$ was opened and water started to run out from the outlet. The outlet water volume was used to measure the flow rates q at different h_n . Graph of q against h_n was plotted to obtain the gradient q/h_n . The permeability could then be calculated using Darcy's law:

$$q = \frac{kA}{\mu} \frac{\rho g h_n}{\Delta l P_{atm}} \quad (4.6)$$

The calculated porosity was 45% and permeability was 23800 mD (Hansen, 2020).

4.2.2 Experimental Procedure

At first, WSPM was poured into the cylinder to a certain height (1130 ml). The composition of Water Based Solution (WBS) used to saturate the porous media is presented in table 2.1. Same WBS was used to completely fill the remaining volume of the cell (250 ml). Until this point, the valve at the bottom had been kept closed.

During the experiment, a known volume of solution (250 ml) was drained out from the bottom of the cylindrical cell and CO₂ was injected from the top simultaneously. The ruler inside the rectangular container was used to continuously monitor the water level as it drained through the bottom valve. The draining process was very careful to prevent any bubbling of air from the bottom into the cell.

After draining out 250 ml WBS, the bottom valve was closed. CO₂ pressure was increased immediately, and the top valve was closed as soon as the desired pressure was attained (5–6 bars). From this point on, the CO₂ pressure decay in the closed system was monitored for 72 hours.

5 Results and Discussion

5.1 Simulation Results and Discussion

Figure 5.1 shows Concentration vs Time graph obtained from the simulation from $t=0$ to $t=72$ hours. The plot is extracted for a point on top of the gas column i.e. at $z=L+H$ to maintain resemblance with experimental setup.

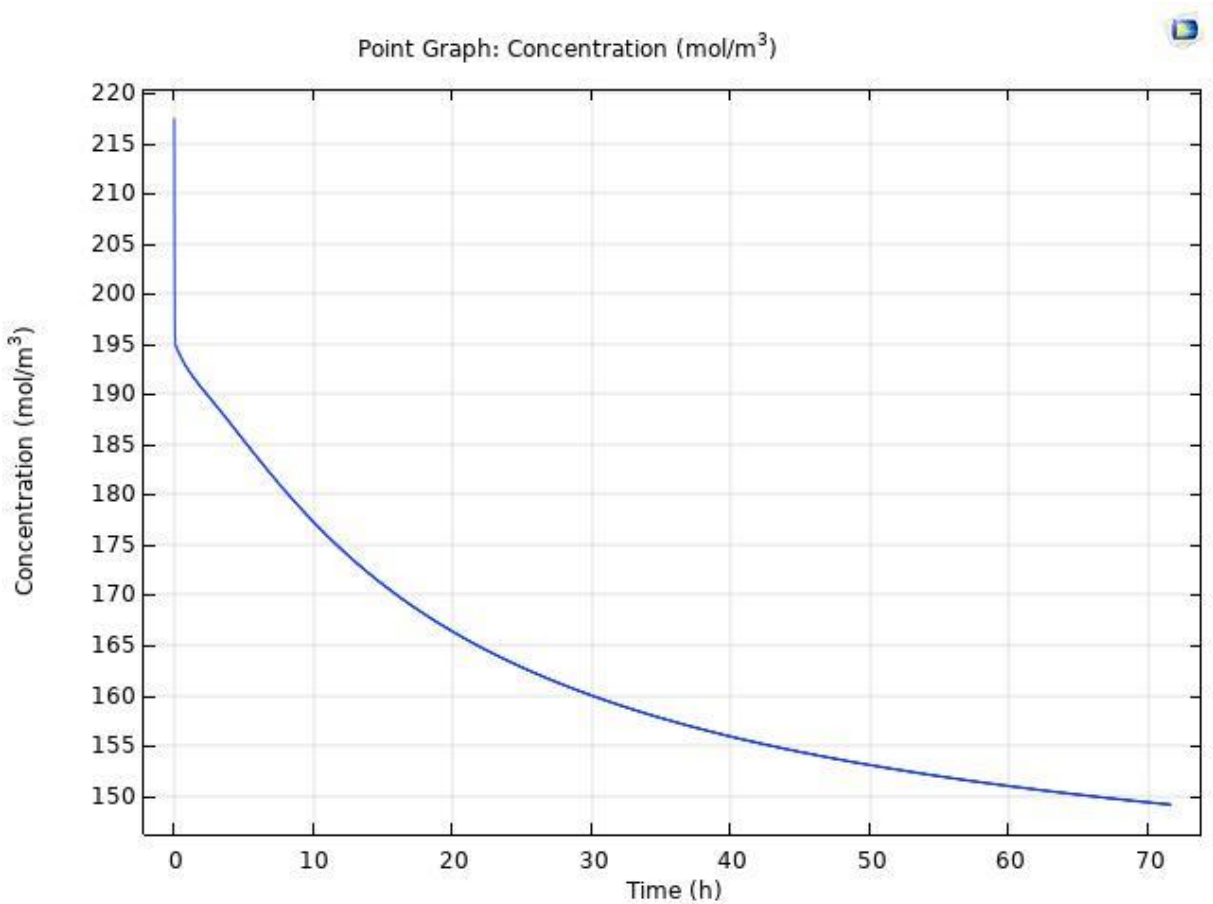


Figure 5.1: Concentration vs Time graph from $t=0$ to $t=72$ hours.

As we can see from the graph, concentration decreases rapidly at initial stages and rate declines with time. The results for $t=0$ to $t=72$ hours were also plotted in terms of Pressure vs Time graph using Microsoft Excel as shown in figure 5.2.

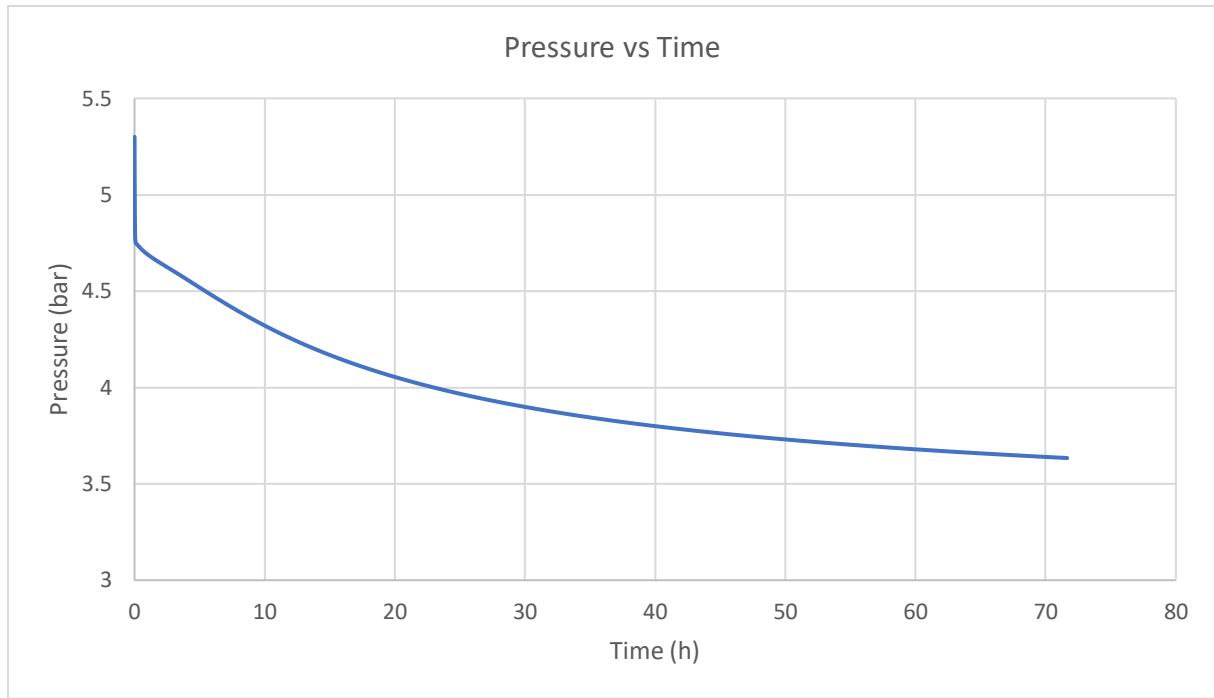


Figure 5.2: Pressure vs Time graph from $t=0$ to $t=72$ hours.

However, even at $t=72$ hours, saturation pressure (P_{eq}) has not been reached and the graph does not become asymptotic. So, the simulation was done for $t=0$ to $t=10000$ hours and Concentration vs Time graph was obtained as shown in figure 5.3.

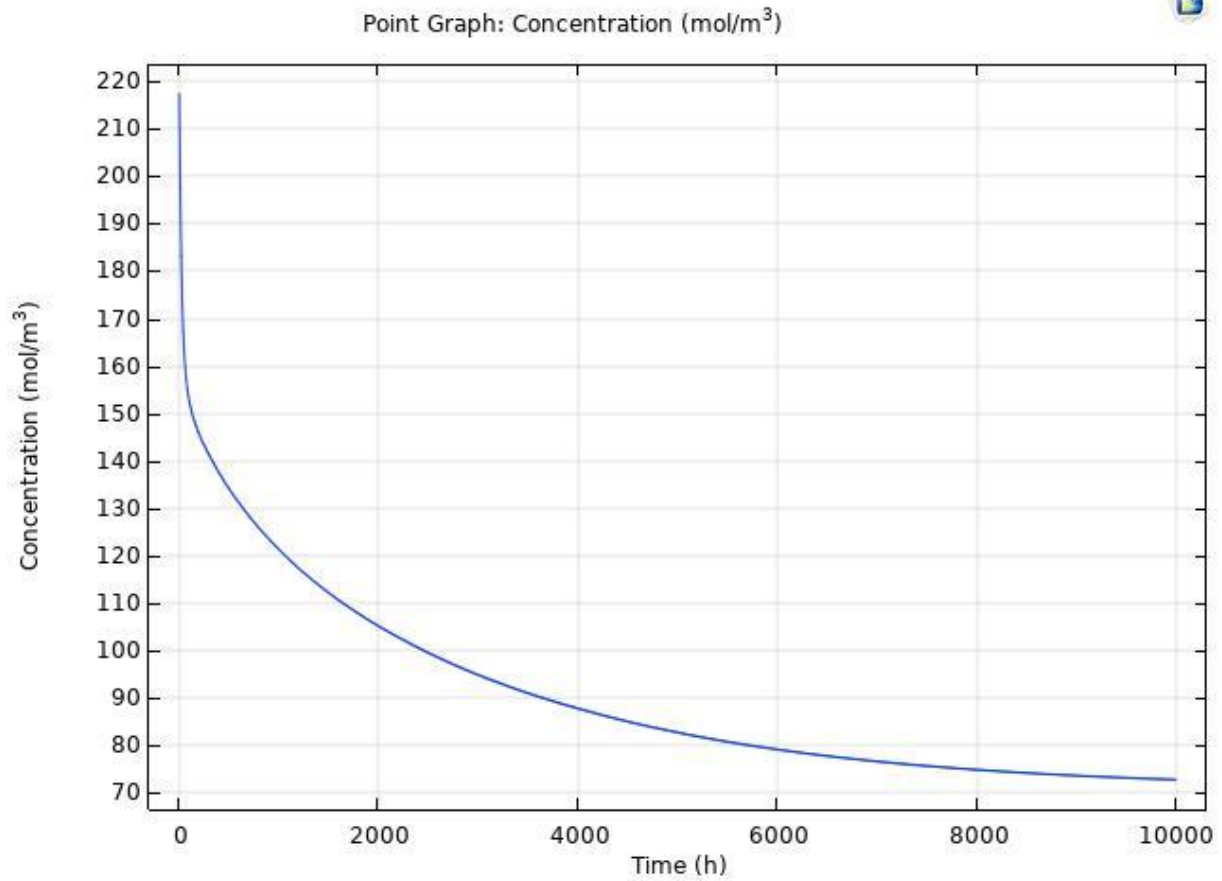


Figure 5.3: Concentration vs Time graph from $t=0$ to $t=10000$ hours.

From figure 5.3, we can see that the graph becomes asymptotic at around $t=10000$ hours. At this point, equilibrium has already been established. Saturation concentration obtained from the graph was 72.63 mol m^{-3} . This corresponds to a saturation pressure (P_{eq}) of 1.77 bar. The value is similar to theoretical saturation pressure (P_{eq}) obtained from the analytical model (Eq. 3.13) i.e 1.78 bar. Table 5.1 shows the parameters used to calculate theoretical P_{eq} including Henry's constant K_{H} obtained from Henry's law and real gas law at initial conditions. Calculation was done in accordance with Eq. 3.13.

Table 5.1: Parameters used for P_{eq} calculation.

Parameter	Value	Unit
P_0	530.065	kPa
h	0.073	m
R	8.314472	$\text{J mol}^{-1} \text{K}^{-1}$
T	293.15	K
K_{H}	2437.387	$\text{m}^3 \text{Pa mol}^{-1}$

z	0.9716	-
L	0.330	m
φ	0.45	-

Graph of $\ln(P(t)-P_{eq})$ was plotted against time in accordance with Eq. 3.11 to obtain a line of best fit. Slopes of tangents at initial and final stages were calculated. The early and late diffusion coefficients were determined from the slopes. Figure 5.4 shows $\ln(P(t)-P_{eq})$ vs Time plot.

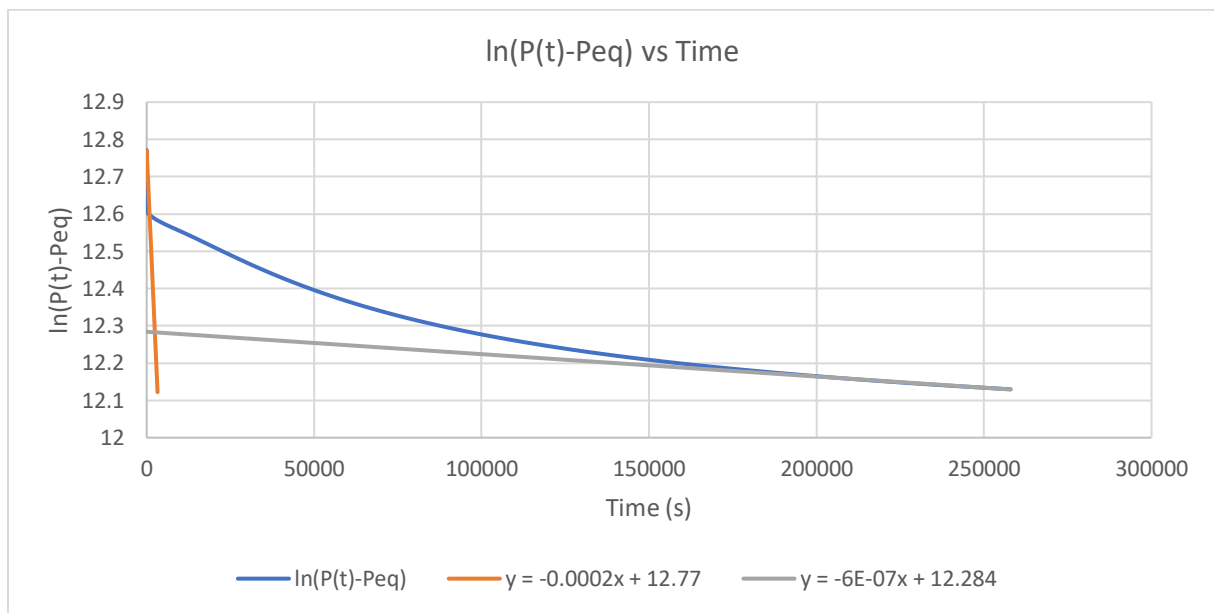


Figure 5.4: $\ln(P(t)-P_{eq})$ vs Time graph

As we can see from the graph, pressure decay gradient is much higher at initial stages compared to later stages. The early and late time diffusion coefficients varied in two orders of magnitude as shown in table 5.2. High diffusivity at earlier stages is can be attributed to the induction of natural convection as a result of density difference between the upper and lower levels of WSPM. At later stages, diffusion coefficient is comparable to the literature value. This is because the diffusion becomes dominant mass transfer mechanism at later stages. It is also noteworthy that the slope is still in the process of decreasing even at $t=72$ hours. And, when calculations were done for diffusivity at $t=1000$ hours, the diffusion coefficient was lamost identical to the literature value. The reduction in diffusivity at later stages is significant in CCS process when investigating the efficiency and viability of chosen underwater reservoirs for sequestration purpose.

Table 5.2: Early and late time diffusion coefficients obtained from simulation.

Diffusion Coefficient	Value	Units
Early	8.8×10^{-6}	$\text{m}^2 \text{s}^{-1}$
Late	2.6×10^{-8}	$\text{m}^2 \text{s}^{-1}$

There is direct proportionality between the pressure decay and mass transfer. The concentration of dissolved gas at the uppermost layer of WSPM bears a significant impact in mass transfer mechanism and hence pressure decay. Figure 5.4 shows three noteworthy stages of mass transfer. There is an initial diffusion state where the uppermost layer of WSPM goes from zero concentration state to fully CO_2 saturated state in a short span of time. Exponential curve fitting done for first 100 seconds of the decay curve indicated exponential initial saturation. After that, the natural convection dominated mass transfer comes into play followed by diffusion dominated mass transfer giving rise to early and late time diffusion coefficients respectively.

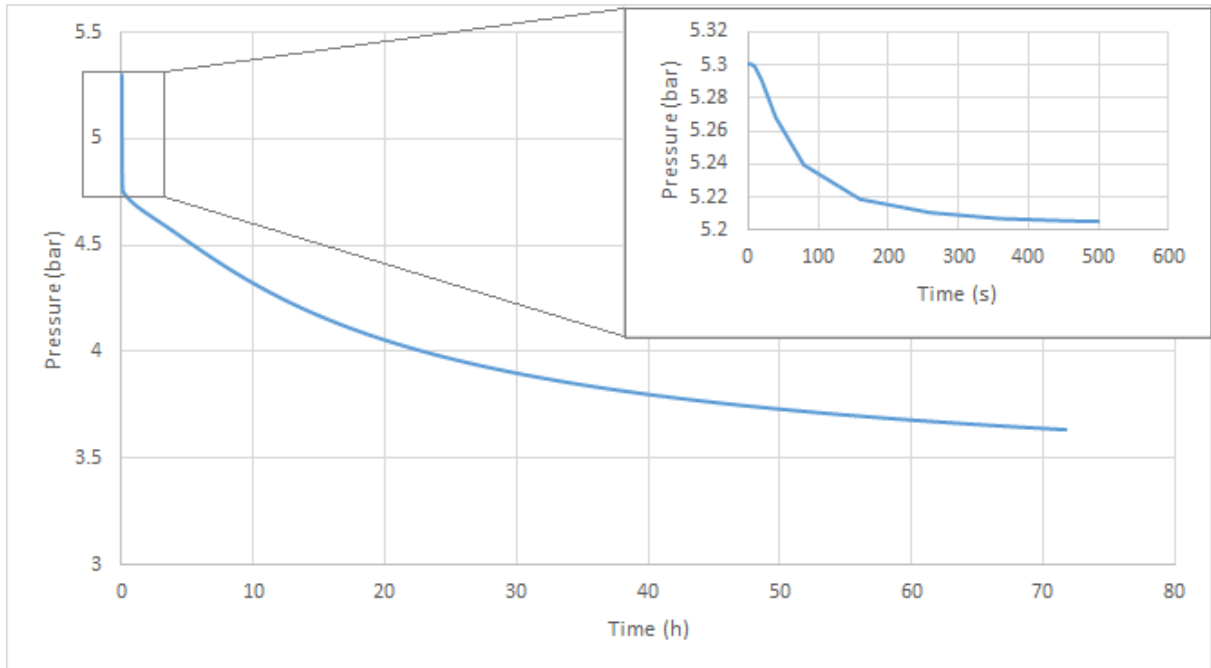


Figure 5.5: Three stages of mass transfer mechanism.

5.1.1 Mixing Regime

The mixing regime in WSPM of 45% porosity and 23800 mD permeability from $t=0$ to $t=23$ hours is shown in figure 5.6-5.9. An instability is observed at $t=0$ s where the CO_2 comes in

contact with WSPM for the first time. The density driven convection is apparent from the pictures showing finger-like displacement. The fingers propagate in the downward direction with time. The mixing regime at later stages are presented in Appendix B where density becomes more uniformly distributed and the fingers start disappearing. Diffusion becomes the dominant mass transfer mechanism at later stages. The simulation is based on porosity and permeability values assumed to be uniform throughout the WSPM. However, some deviation can be expected in practical scenarios where porosity and permeability are also functions of the type of material used. Due to flow resistivity posed by the porous medium, no vortices are seen as would have been in the case involving only water. Also, downward propagation is seen dominant compared to radial propagation at initial stages. However, merging occurs at later stages giving rise to a more uniform density distribution.

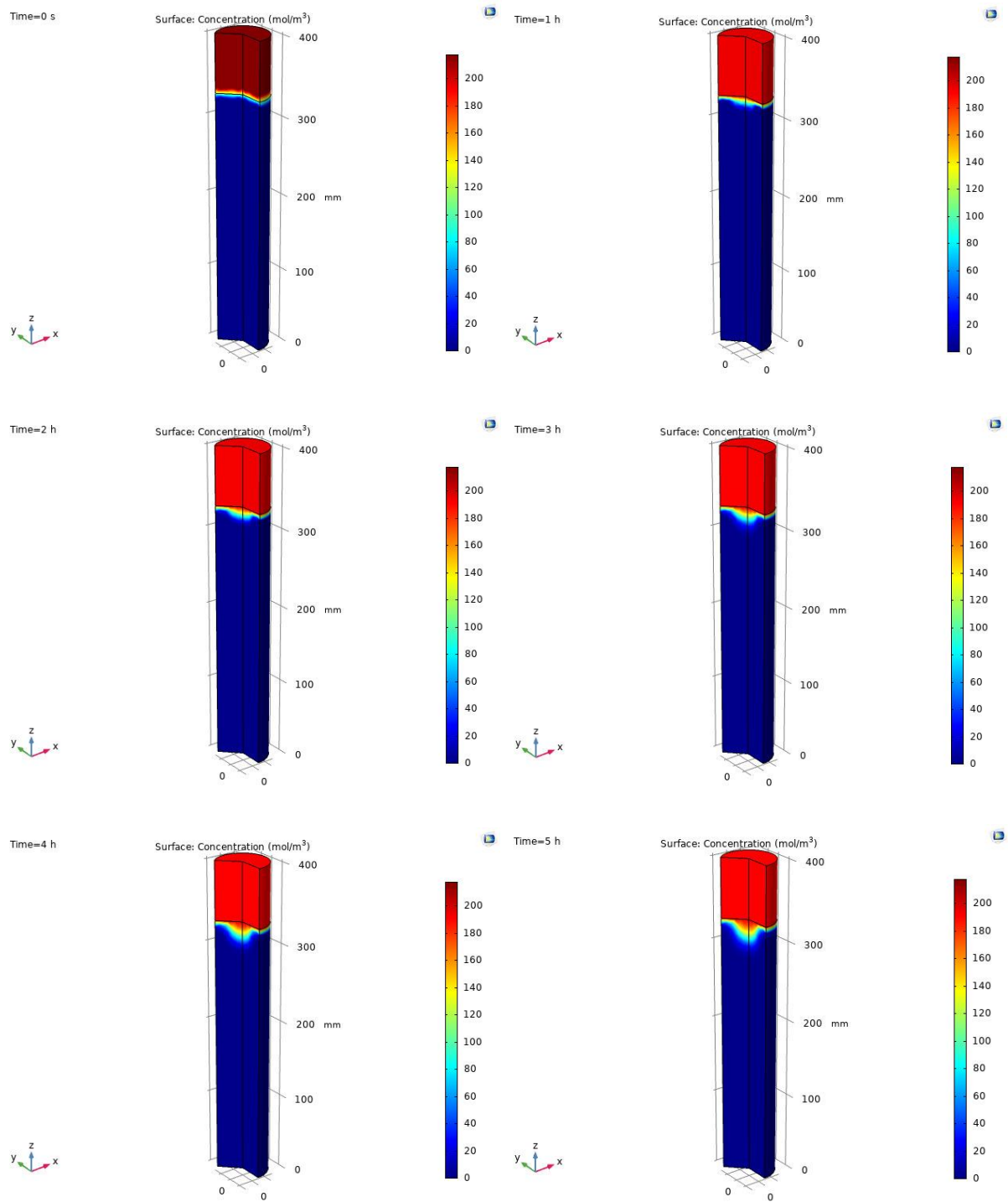


Figure 5.6: Mixing regime in WSPM of 45% porosity and 23800 mD permeability from $t=0$ to $t=5$ hours.

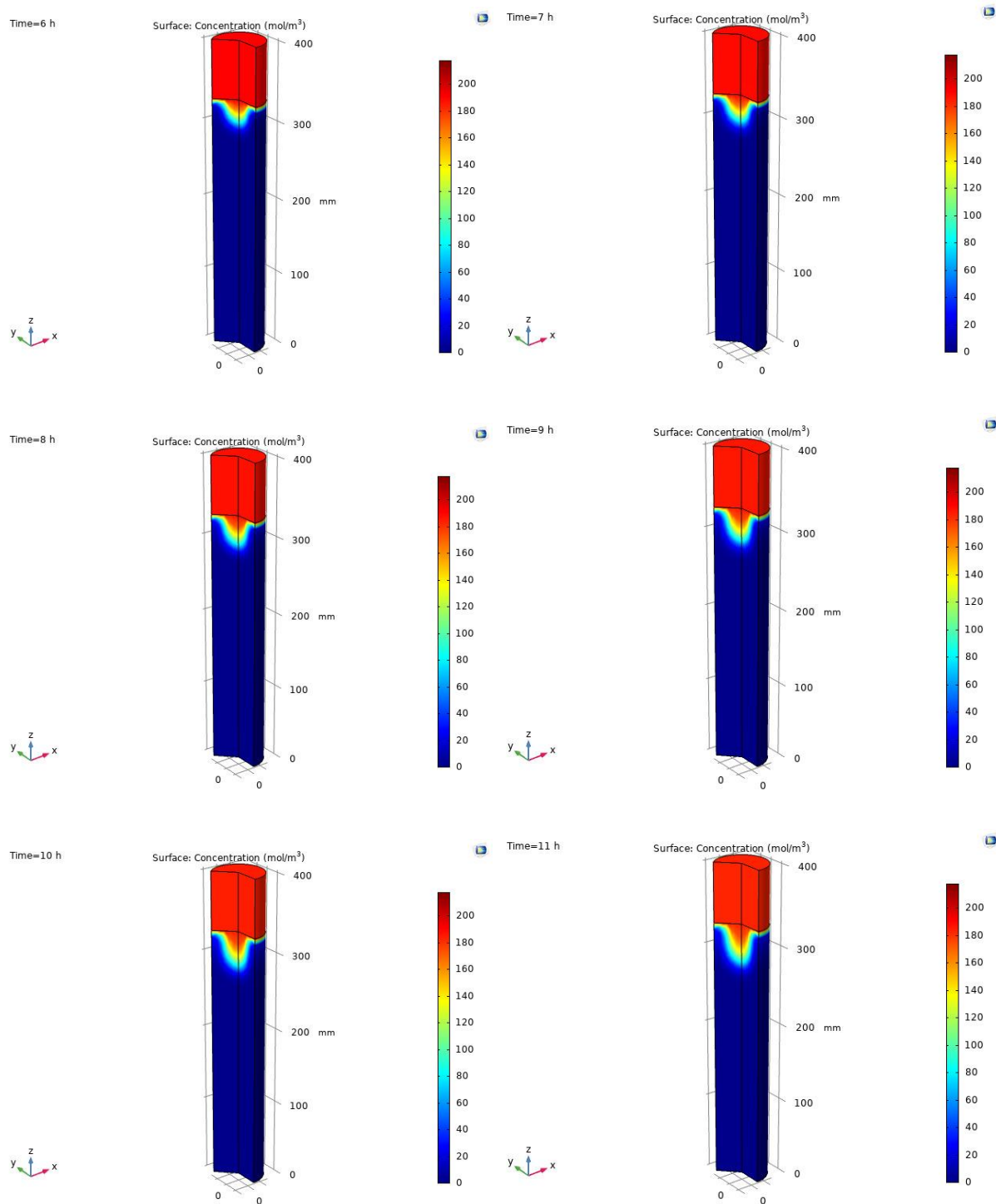


Figure 5.7: Mixing regime in WSPM of 45% porosity and 23800 mD permeability from $t=6$ to $t=11$ hours.

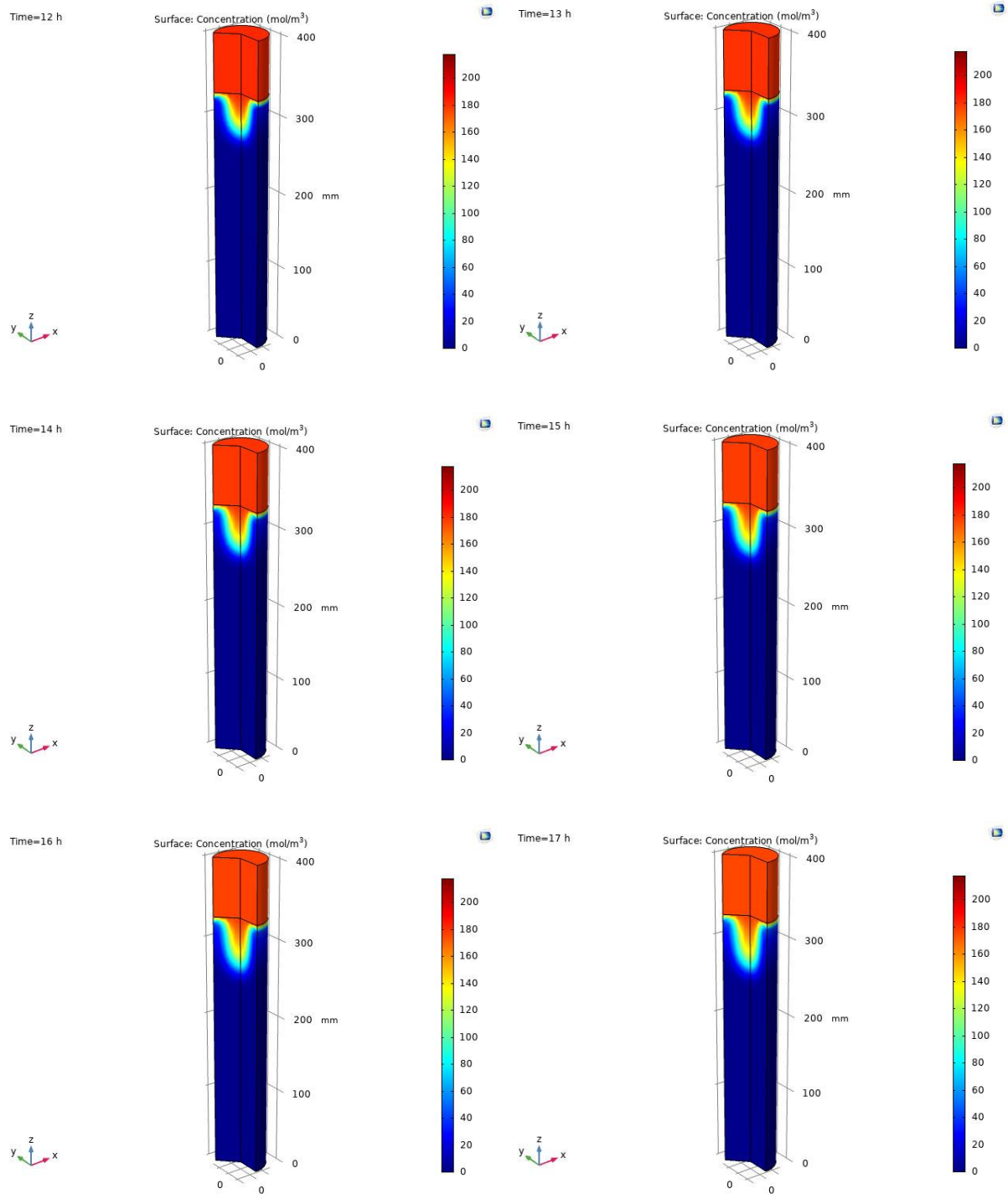


Figure 5.8: Mixing regime in WSPM of 45% porosity and 23800 mD permeability from $t=12$ to $t=17$ hours.

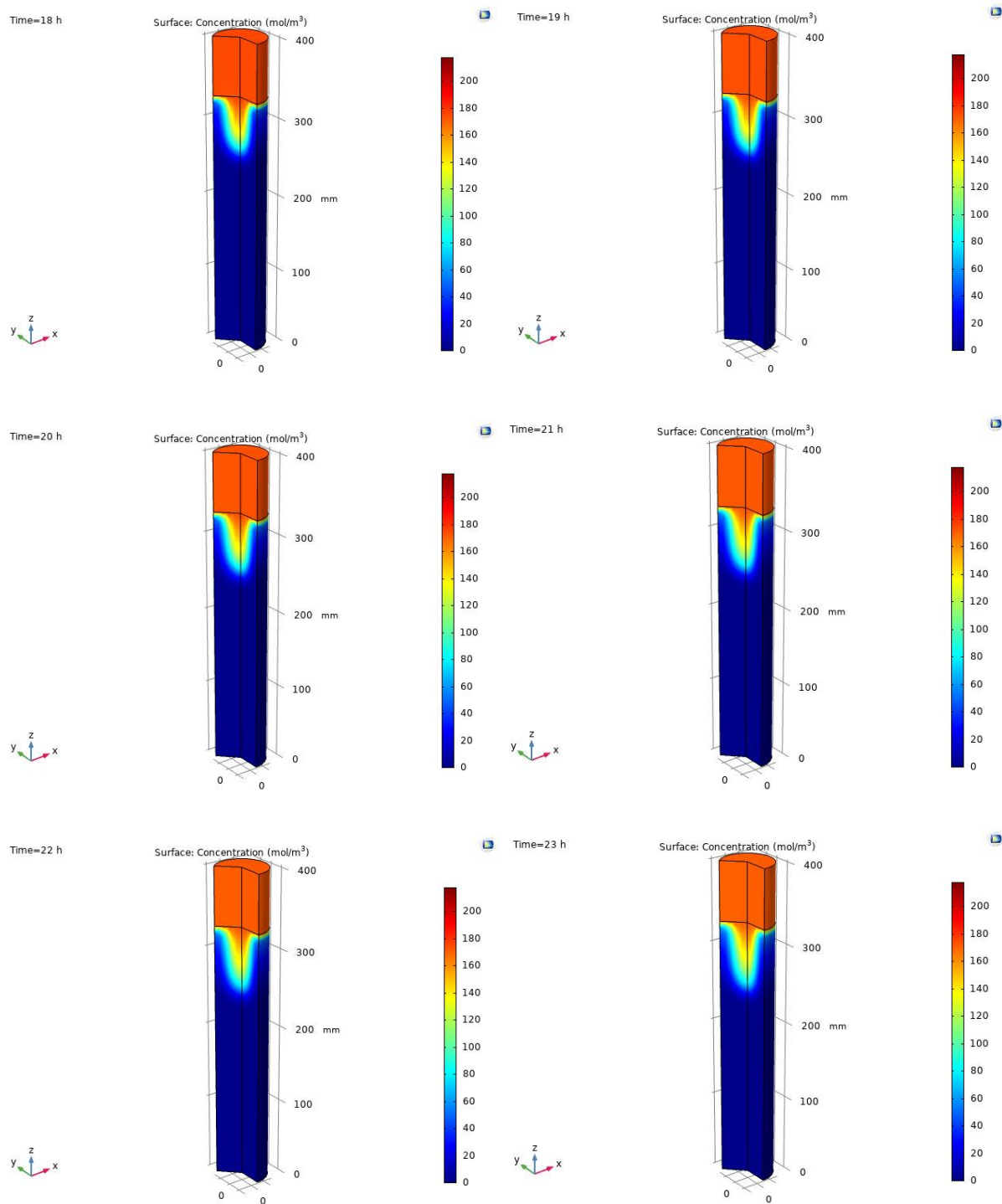


Figure 5.9: Mixing regime in WSPM of 45% porosity and 23800 mD permeability from t=18 to t=23 hours.

5.2 Experimental Results

Figure 5.10 shows pressure decay curve obtained from experimental results. The curve is similar to the one obtained from simulation. There is decrease in the rate of CO₂ consumption with time. As discussed earlier, the higher rate at initial stages can be attributed to natural convection dominated flow regime.

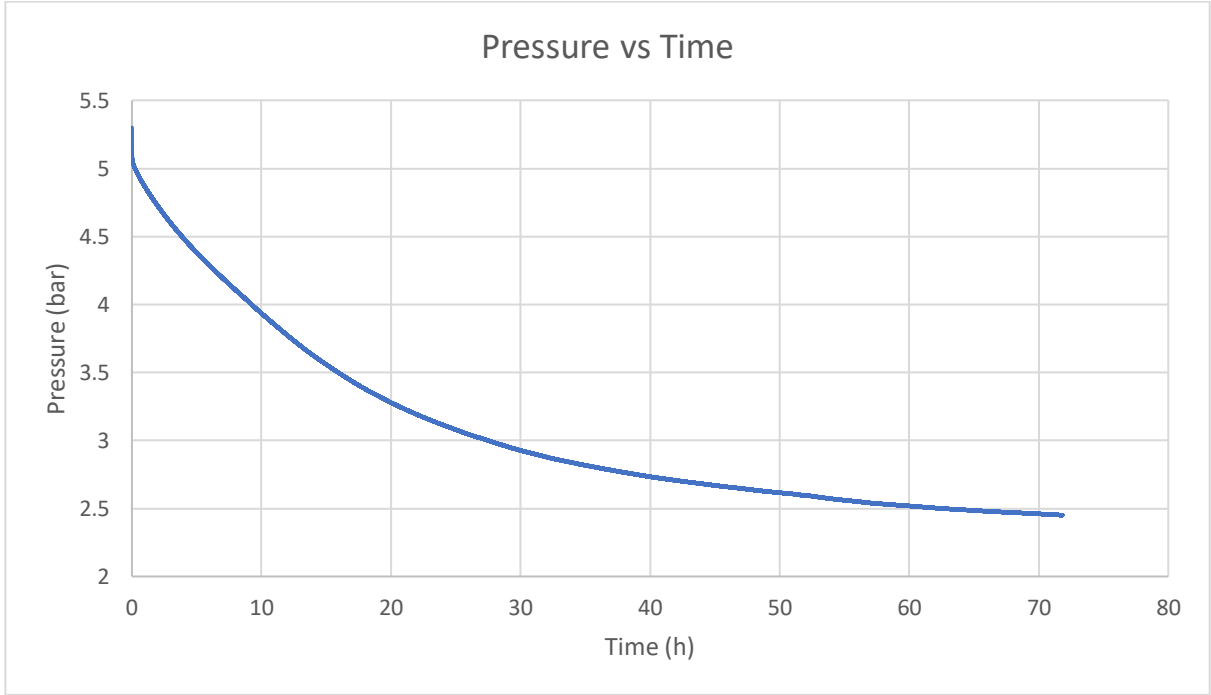


Figure 5.10: Experimental Pressure Decay Curve

It is noteworthy that there is some discrepancy in pressure values towards the end compared to the simulation. This might have been as a result of some undetected leakage which could make significant impact in experiments involving high gas pressure for a considerable duration. Due to time limitations, caused by numerous failed trials before this one, the experiment could not be repeated. However, the trend shown by the graph was as anticipated. Extrapolation of the curve shows that if the experiment had been conducted for longer duration, it is very likely to reach the theoretical saturation pressure P_{eq} .

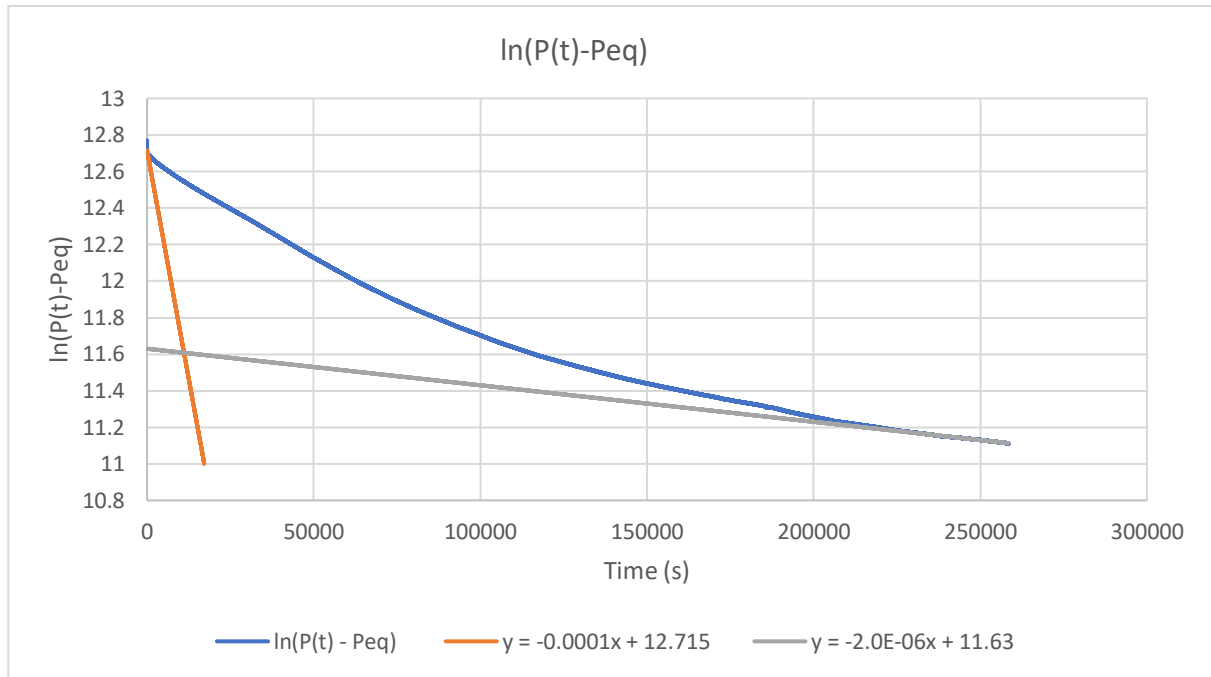


Figure 5.11: $\ln(P(t)-P_{eq})$ vs Time graph from the experiment.

The early and late time diffusion coefficients were calculated from the slopes of tangents from $\ln(P(t)-P_{eq})$ vs time plot as shown in figure 5.11. The values are presented in table 5.3. As in the simulation, early and late time diffusion coefficients calculated in accordance with Eq. 3.11 varied in two orders of magnitude. As discussed earlier, natural convection is a dominant mass transfer mechanism at earlier stages and pure diffusion becomes dominant at later stages when density becomes more uniform as the function of space. The diffusivity at later stages is quite comparable to the literature value as in the case of simulation results. Also, curve has not become asymptotic in a relatively short span of the experiment. Hence, if allowed to run for long duration, it is expected that the value of diffusion coefficient will be close to literature value.

Table 5.3: Early and late time diffusion coefficients obtained from experimental results.

Diffusion Coefficient	Value	Units
Early	4.4×10^{-6}	$m^2 s^{-1}$
Late	8.8×10^{-8}	$m^2 s^{-1}$

Figure 5.12 shows three stages of mass transfer mechanism as was seen in the simulation results. The first diffusion state lasts for only a short interval of time as expected where the uppermost layer of WSPM becomes saturated by CO_2 gas. The second stage of mass transfer is dominated

by density-driven natural convection occurring as a result of density difference across the fluid volume and an instability caused by gravitational effects. Finger like mixing regime is observed. During the third stage, diffusion becomes the dominant mass transfer mechanism when the fluid becomes relatively stable in terms of spatial density variance.

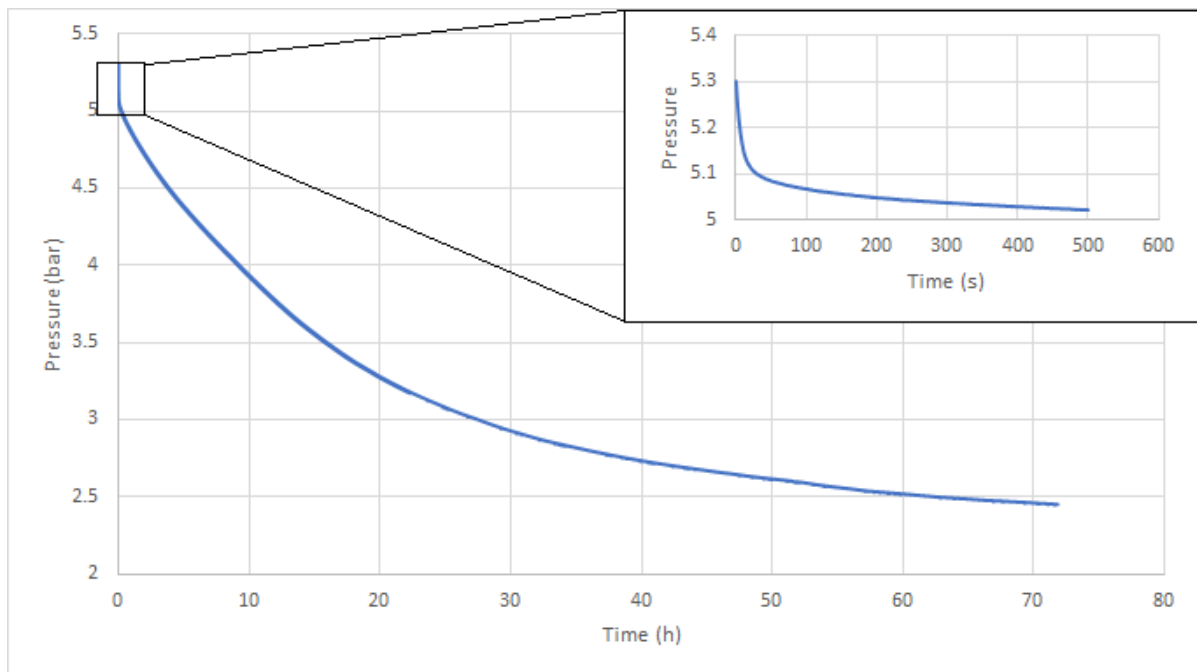


Figure 5.12: Three stages of mass transfer mechanism (experimental).

5.2.1 Mixing Regime (Experimental)

The propagation of yellow area was captured over time using two cameras placed at 90 degrees angle with one another. The photographs taken at different time intervals are shown in figure 5.13–5.16. The occurrence of yellow color is due to CO_2 gas reacting with NaOH in the solution and is indicated by Bromothymol Blue indicator. The mixing regime is difficult to view in detail because of the limited amount of blue liquid present in the interparticle spaces between the glass beads. Also, the concentration profile is not as distinct as in the simulation because slight variations in color cannot be seen. The mixing regime was similar to the simulation results. The occurrence of fingering as a result of density-driven convection was visible. There was more than one finger like displacements. This might be as a result of uneven surface between the phases which is not taken into consideration in the simulation. Also, the medium is not uniform regarding the porosity and permeability as is assumed in the simulation. The finger progression seems faster compared to the simulation results, but this can be because the slightest amount of CO_2 could affect the color change compared to the simulation where the concentration profile

is seen in a continuous spectrum. However, more experiments must be performed to reach a conclusion.

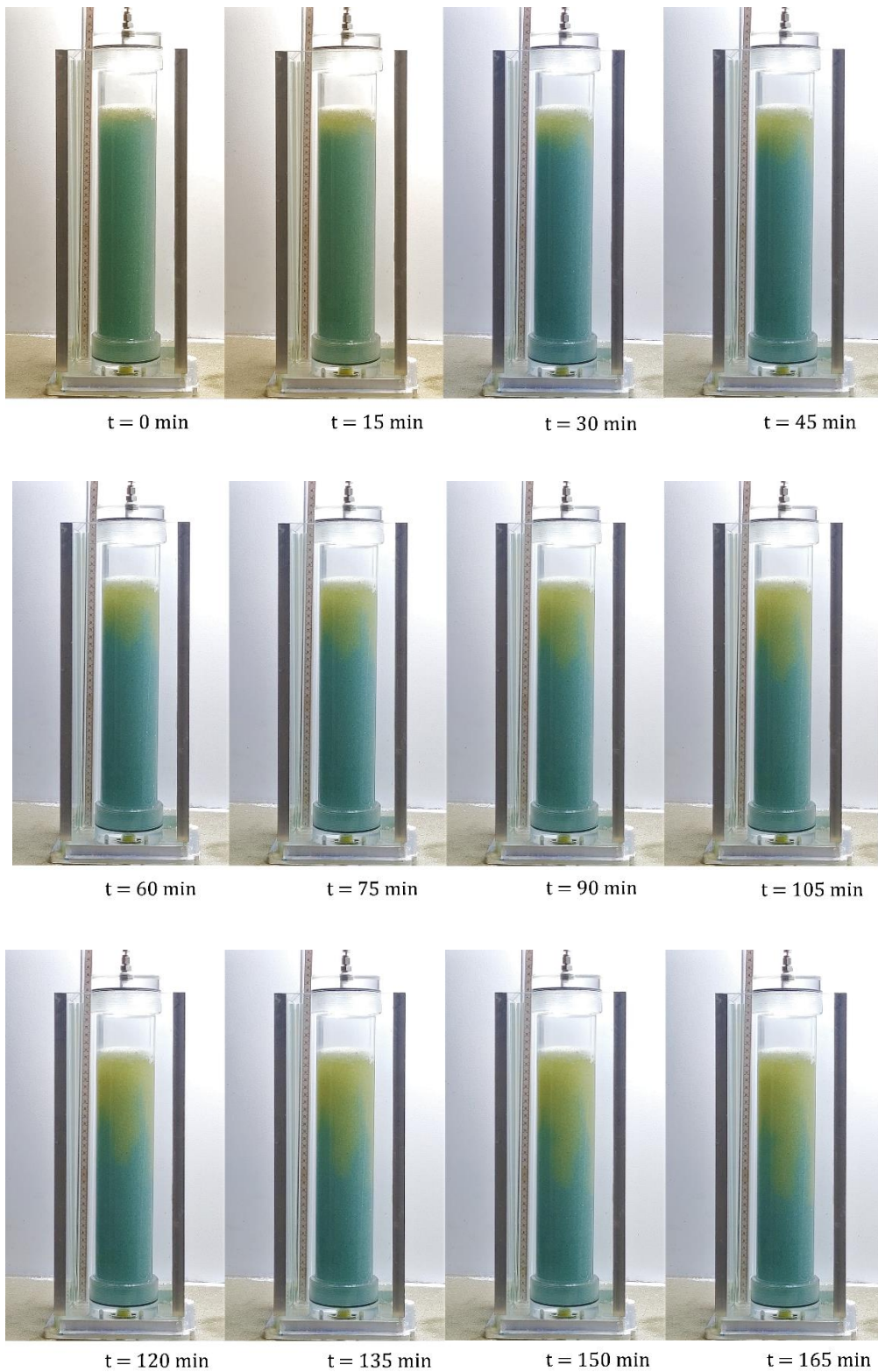


Figure 5.13: Mixing regime from experiment in WSPM of 45% porosity and 23800 mD permeability from $t=0 \text{ min}$ to $t=165 \text{ min}$ (Camera 1: Google Pixel 4a).

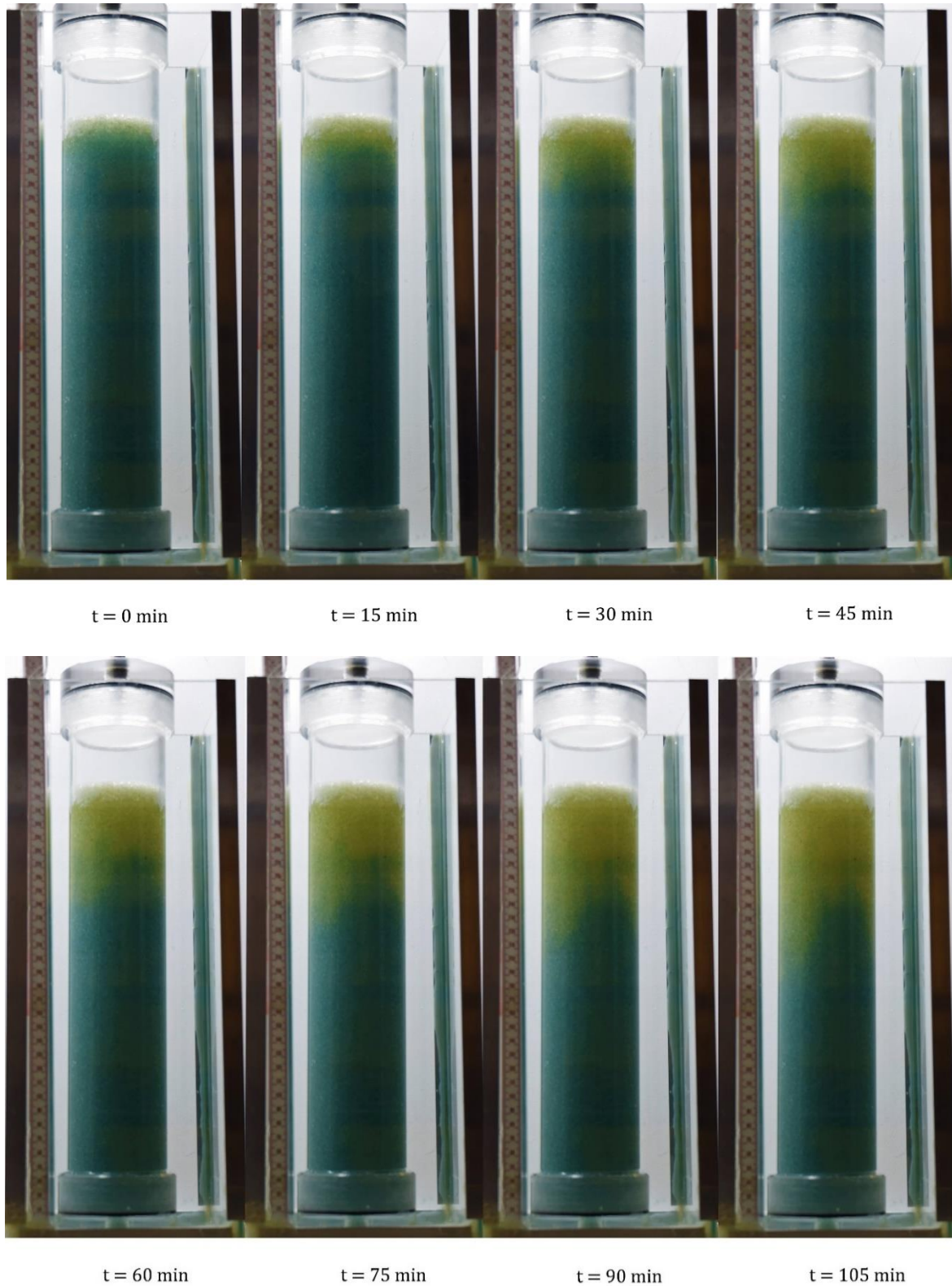
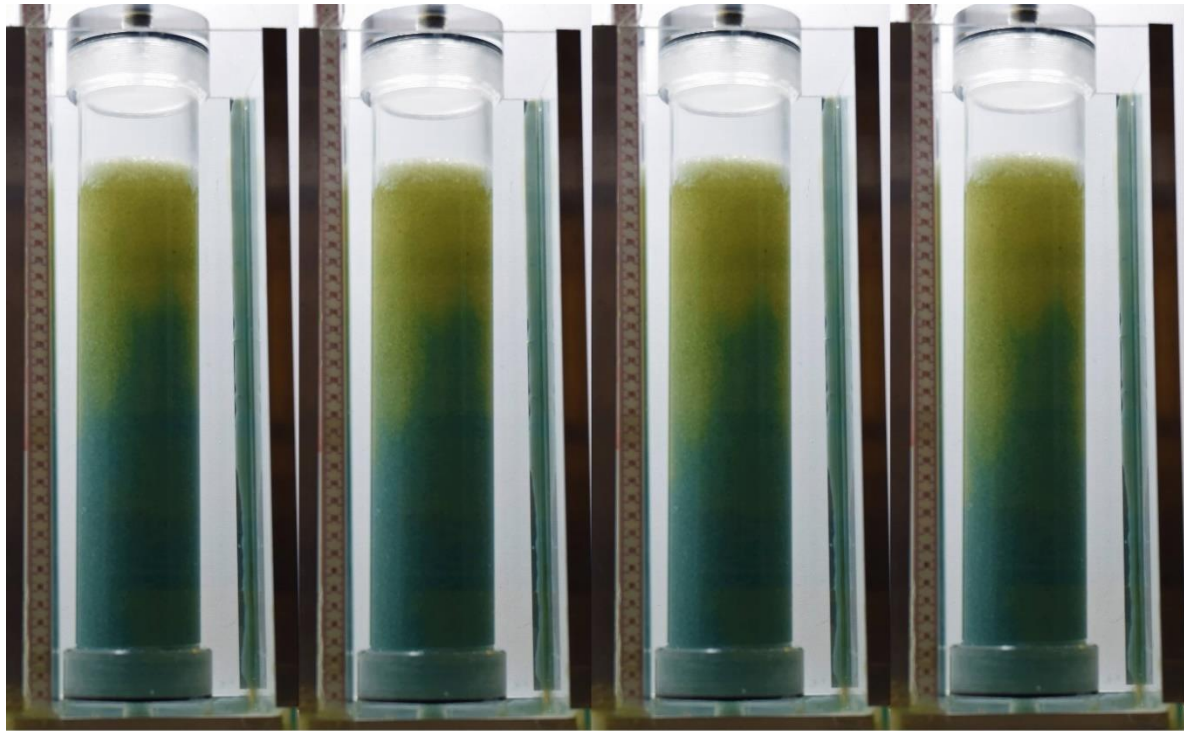


Figure 5.14: Mixing regime from experiment in WSPM of 45% porosity and 23800 mD permeability from $t=0$ min to $t=105$ min (Camera 2: Nikon D5300).

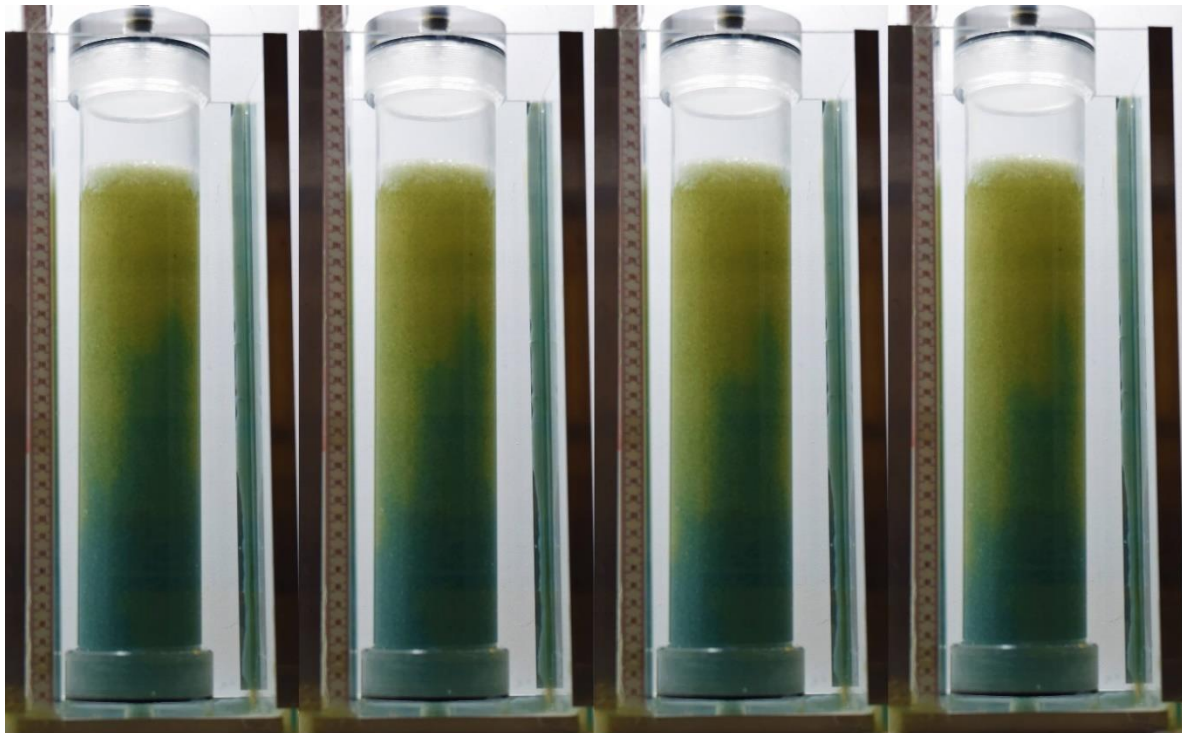


t = 120 min

t = 135 min

t = 150 min

t = 165 min



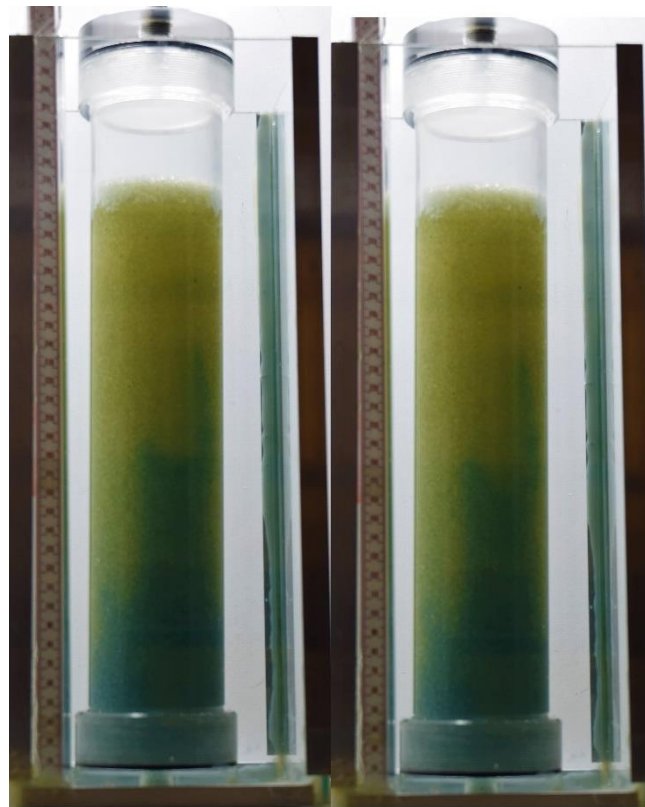
t = 180 min

t = 195 min

t = 210 min

t = 225 min

Figure 5.15: Mixing regime from experiment in WSPM of 45% porosity and 23800 mD permeability from t=120 min to t=225 min (Camera 2: Nikon D5300).



t = 240 min

t = 255 min

Figure 5.16: Mixing regime from experiment in WSPM of 45% porosity and 23800 mD permeability from t=240 min to t=255 min (Camera 2: Nikon D5300).

6 Conclusion

The study of CO₂ absorption and mass transfer mechanisms in Water Saturated Porous Media (WSPM) was done through simulation using COMSOL Multiphysics® software and pressure decay experiment conducted using glass beads of 1 mm diameter resembling a uniformly distributed porous medium.

An analytical model was established using suitable boundary conditions based on previously done pressure decay studies. The study was done in a closed PVT cell partially filled with WSPM and partially with pressurized CO₂ gas. The dimensions of the cylindrical cell, gas column and matrix volume were consistent with the experimental setup. Pressure decay due to absorption into the WSPM was monitored over time in the closed system. The pressure decay curves obtained from the simulation and the experiment were used to obtain early and late time diffusion coefficients and the values were compared with literature value. Also, the saturation pressure obtained from the simulation was compared with the one obtained from the theoretical model. The study was focused in analyzing the contribution of density-driven natural convection in mass transfer mechanism at early and late stages of the absorption process.

Both simulation and experimental data showed similar trend regarding the pressure decay. Calculated early time diffusion coefficients were two orders of magnitude higher than late diffusion coefficients in both the simulation and the experiment. The effect of density driven natural convection was apparent from high diffusivity obtained at early stages. At later stages, the diffusivity values were quite comparable to literature value. Although saturation pressure was not reached in the limited time frame the experiment was conducted, simulation results at long time duration showed saturation pressure almost similar to the value obtained from the analytical model.

Three stages of diffusivity could be observed from pressure decay curves of both the simulation and the experiment. The initial stage lasted for a very short interval of time where rapid pressure decline was observed as a result of absorption by the uppermost layer of WSPM to establish an equilibrium with the gas phase. After that, the density-driven natural convection became the dominant mass transfer mechanism giving rise to the diffusivity value almost two orders of magnitude higher than the literature value. At the final stage, when a relatively uniform density distribution was established in relation to spatial function, pure diffusion became the dominant mass transfer mechanism with diffusivity very close to literature value. Finger propagation

observed in the mixing regime was mainly in downward direction before expanding horizontally.

The study of diffusivity and saturation pressure can be very significant for sequestration of CO₂ in deep sea geological formations. Further investigation into the subject is deemed crucial in assessing the efficiency and viability of underwater reservoirs for sequestration process.

References

- Adnan, A. I., Ong, M. Y., Nomanbhay, S., & Show, P. L. (2020). Determination of Dissolved CO₂ Concentration in Culture Media: Evaluation of pH Value and Mathematical Data. *Processes*, 8(11). <https://doi.org/10.3390/pr8111373>
- Anna, P. de, Jimenez-Martinez, J., Tabuteau, H., Turuban, R., Le Borgne, T., Derrien, M., & Méheust, Y. (2014). Mixing and reaction kinetics in porous media: An experimental pore scale quantification. *Environmental Science & Technology*, 48(1), 508–516.
- Battiato, I., V, P., Malley, D., Miller, C., Takhar, P., Valdes-Parada, F., & Wood, B. (2019). Theory and Applications of Macroscale Models in Porous Media. *Transport in Porous Media*, 130. <https://doi.org/10.1007/s11242-019-01282-2>
- COMSOL Multiphysics® (5.4). (2018). [Computer software]. COMSOL AB. www.comsol.com
- Cushman, J. H. (1990). Dynamics of Fluids in Hierarchical Porous Media Academic Press. *San Diego, California*.
- Cushman, John H., Bennethum, L. S., & Hu, B. X. (2002). A primer on upscaling tools for porous media. *Advances in Water Resources*, 25(8–12), 1043–1067.
- Diffusion. (2021). <https://chem.libretexts.org/@go/page/1392>
- Diffusion Equation: Fick's Laws of Diffusion. (n.d.). Retrieved May 24, 2021, from <https://www.comsol.com/multiphysics/diffusion-equation?parent=diffusion-0402-392-412>
- Erga, O., Juliussen, O., & Lidal, H. (1995). Carbon dioxide recovery by means of aqueous amines. *Energy Conversion and Management*, 36(6–9), 387–392.
- Farajzadeh, R., Barati, A., Delil, H. A., Bruining, J., & Zitha, P. L. J. (2007). Mass Transfer of CO₂ Into Water and Surfactant Solutions. *Petroleum Science and Technology*, 25(12), 1493–1511. <https://doi.org/10.1080/10916460701429498>
- Farajzadeh, Rouhollah. (2009). *Enhanced transport phenomena in CO₂ sequestration and CO₂ EOR*.
- Gmelin, L. (1968). *Gmelins Handbuch der anorganischen chemie* (Issue 57). Verlag Chemie gmbh.
- Hansen, T. (2020). *An Experimental Study of the Enhanced Mass Transfer Process by CO₂ Absorption for Carbon Storage in Saline Aquifers* [Master's Thesis]. University of Stavanger.
- IEA, I. (2011). Clean Energy Progress Report. *International Energy Agency. Paris*, 72.

- Jiménez-Martínez, J., Anna, P. de, Tabuteau, H., Turuban, R., Borgne, T. L., & Méheust, Y. (2015). Pore-scale mechanisms for the enhancement of mixing in unsaturated porous media and implications for chemical reactions. *Geophysical Research Letters*, *42*(13), 5316–5324.
- Khosrokhavar, R., Elsinga, G., Farajzadeh, R., & Bruining, H. (2014). Visualization and investigation of natural convection flow of CO₂ in aqueous and oleic systems. *Journal of Petroleum Science and Engineering*, *122*, 230–239. <https://doi.org/10.1016/j.petrol.2014.07.016>
- Knoche, W. (1980). Chemical reactions of CO₂ in water. In *Biophysics and physiology of carbon dioxide* (pp. 3–11). Springer.
- Lage, J. L., De Lemos, M. J. S., & Nield, D. A. (2002). 8—Modeling Turbulence in Porous Media. In Derek B. Ingham & I. Pop (Eds.), *Transport Phenomena in Porous Media II* (pp. 198–230). Pergamon. <https://doi.org/10.1016/B978-008043965-5/50009-X>
- Lapwood, E. R. (1948). Convection of a fluid in a porous medium. *Mathematical Proceedings of the Cambridge Philosophical Society*, *44*(4), 508–521. Cambridge Core. <https://doi.org/10.1017/S030500410002452X>
- Lindeberg, E., & Wessel-Berg, D. (1997). Vertical convection in an aquifer column under a gas cap of CO₂. *Energy Conversion and Management*, *38*, S229–S234.
- Merrikh, A. A., & Lage, J. L. (2005). 3—From Continuum to Porous–Continuum: The Visual Resolution Impact on Modeling Natural Convection in Heterogeneous Media. In D. B. Ingham & I. Pop (Eds.), *Transport Phenomena in Porous Media III* (pp. 60–96). Pergamon. <https://doi.org/10.1016/B978-008044490-1/50007-7>
- Models.ssf.buoyancy_darcy_elder.pdf* (n.d.). Retrieved May 24, 2021, from https://www.comsol.com/model/download/839361/models.ssf.buoyancy_darcy_elder.pdf
- Mofarahi, M., Khojasteh, Y., Khaledi, H., & Farahnak, A. (2008). Design of CO₂ absorption plant for recovery of CO₂ from flue gases of gas turbine. *Energy*, *33*(8), 1311–1319. <https://doi.org/10.1016/j.energy.2008.02.013>
- Moghaddam, R. N., Rostami, B., Pourafshary, P., & Fallahzadeh, Y. (2012). Quantification of density-driven natural convection for dissolution mechanism in CO₂ sequestration. *Transport in Porous Media*, *92*(2), 439–456.
- Mojtaba, S., Behzad, R., Rasoul, N. M., & Mohammad, R. (2014). Experimental study of density-driven convection effects on CO₂ dissolution rate in formation water for geological storage. *Journal of Natural Gas Science and Engineering*, *21*, 600–607. <https://doi.org/10.1016/j.jngse.2014.09.020>

- Moulu, J. C. (1989). Solution-gas drive: Experiments and simulation. *Journal of Petroleum Science and Engineering*, 2(4), 379–386.
- Peng, X. F., & Wu, H. L. (2005). 14—Pore-Scale Transport Phenomena in Porous Media. In D.B. Ingham & I. Pop (Eds.), *Transport Phenomena in Porous Media III* (pp. 366–398). Pergamon. <https://doi.org/10.1016/B978-008044490-1/50018-1>
- Posch, S., & Haider, M. (2013). Dynamic modeling of CO₂ absorption from coal-fired power plants into an aqueous monoethanolamine solution. *Chemical Engineering Research and Design*, 91(6), 977–987. <https://doi.org/10.1016/j.cherd.2012.09.016>
- Raabe, D. (2004). Overview of the lattice Boltzmann method for nano- and microscale fluid dynamics in materials science and engineering. *Modelling and Simulation in Materials Science and Engineering*, 12(6), R13.
- Riazi, M. R. (1996). A new method for experimental measurement of diffusion coefficients in reservoir fluids. *Journal of Petroleum Science and Engineering*, 14(3), 235–250. [https://doi.org/10.1016/0920-4105\(95\)00035-6](https://doi.org/10.1016/0920-4105(95)00035-6)
- Statistics, I. E. A. (2011). CO₂ emissions from fuel combustion-highlights. *IEA, Paris* <Http://Www.Iea.Org/Co2highlights/Co2highlights.Pdf>. Cited July.
- Walter, F. (2013). COMSOL Blog. *Meshing Considerations for Linear Static Problems*. <https://www.comsol.com/blogs/meshing-considerations-linear-static-problems/>
- What Is Convection?* (n.d.). Retrieved May 24, 2021, from <https://www.comsol.com/multiphysics/what-is-convection?parent=fluid-flow-heat-transfer-and-mass-transport-0402-382>
- Xiao, F. (2013a). *Pore-scale simulation frameworks for flow and transport in complex porous media*. Colorado School of Mines.
- Xiao, F. (2013b). *Pore-scale simulation frameworks for flow and transport in complex porous media*. Colorado School of Mines.
- Yang, C., & Gu, Y. (2006). Accelerated mass transfer of CO₂ in reservoir brine due to density-driven natural convection at high pressures and elevated temperatures. *Industrial & Engineering Chemistry Research*, 45(8), 2430–2436.
- Zhang, Y. P., Hyndman, C. L., & Maini, B. B. (2000). Measurement of gas diffusivity in heavy oils. *Journal of Petroleum Science and Engineering*, 25(1), 37–47. [https://doi.org/10.1016/S0920-4105\(99\)00031-5](https://doi.org/10.1016/S0920-4105(99)00031-5)

Appendix A

Create new file by choosing **New** from **File** menu.

Model Wizard

1. Choose **2D Axysymmetric** in Model Wizard window.
2. Under **Select Physics**, select **Fluid Flow>Porous Media** and **Subsurface Flow>Darcy's Law (dl)**.
3. Click **Add**
4. Again, under **Select Physics**, select **Chemical Species Transport>Transport of Diluted Species (tds)**.
5. Click **Add**.
6. Click **Study**.
7. Now, under **Select Study**, select **General Studies>Time Dependent**.
8. Click **Done**.

Global Definitions

1. In **Model Builder** window, click **Parameters 1** under **Global Definitions**.
2. Under **Parameters>Settings**, enter the following settings:

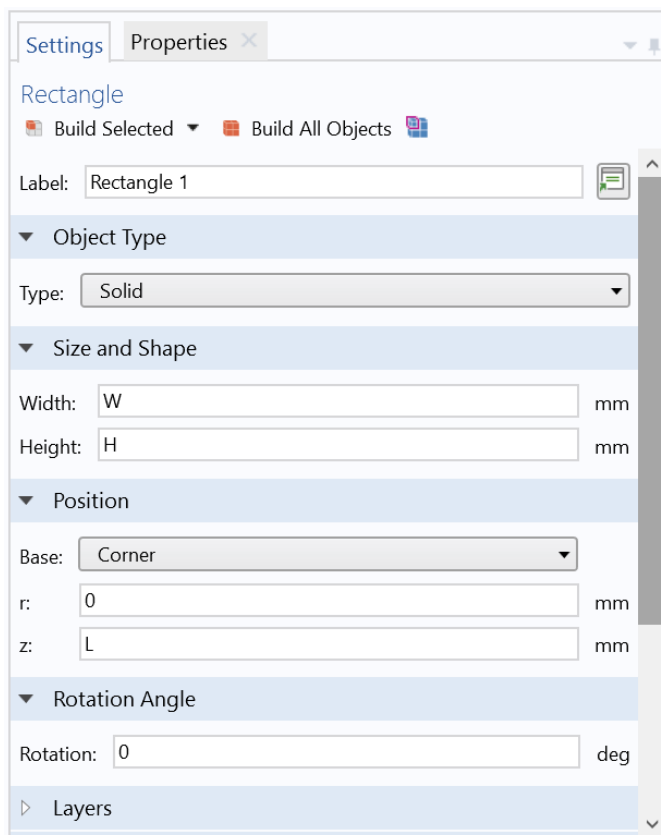
Name	Expression	Value	Description
rho0	1000[kg/m^3]	1000 kg/m ³	Pristine water density
c0	0[mol/m^3]	0 mol/m ³	Initial CO2 concentration in WSPM
c_s	217.47[mol/m^3]	217.47 mol/m ³	Initial CO2 concentration in gas column
beta	0.044[kg/mol]	0.044 kg/mol	Increase in density due to CO2 concentration
p0	0[atm]	0 Pa	Reference pressure
mu	1.0020e-3[Pa*s]	0.001002 Pa*s	Dynamic viscosity
kappa	23.8[D]	7.9388E-29 C*m	Permeability

epsilon	0.45	0.45	Porosity
D_L	1.6e-9[m^2/s]	1.6E-9 m^2/s	Molecular diffusion
R0	8.3145[J/(mol*K)]	8.3145 J/(mol·K)	Universal gas constant
T	293.15[K]	293.15 K	Temperature
L	330[mm]	0.33 m	Height of water column
W	33[mm]	0.033 m	Radius of the PVT cell
H	73[mm]	0.073 m	Height of gas column

Geometry

Rectangle 1 (r1)

1. In the **Geometry** toolbar, click **Primitives>Rectangle**.
2. In the **Settings** window for **Rectangle 1**, enter the following settings:



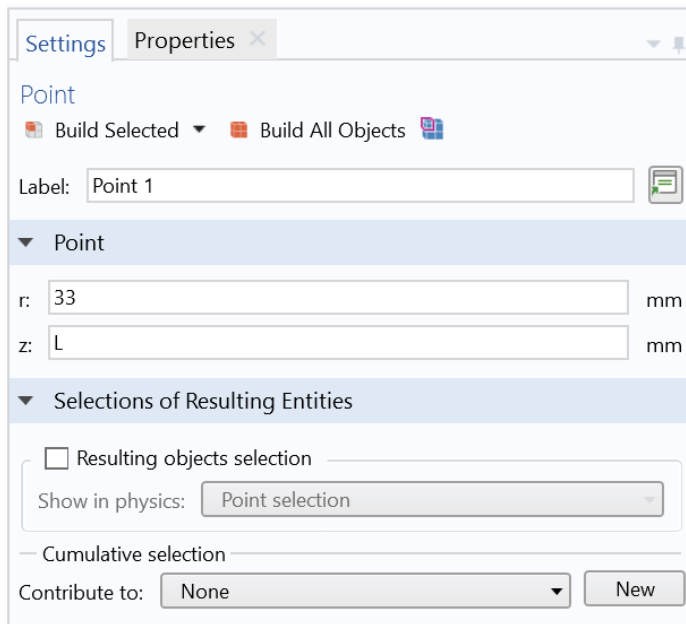
Rectangle 2 (r2)

1. In the **Geometry** toolbar, click **Primitives>Rectangle**.
2. In the **Settings** window for **Rectangle 2**, enter the following settings:



Point 1 (pt 1)

1. In the **Geometry** toolbar, click **Primitives>Point**.
2. In the **Settings** window for **Point 1**, enter the following settings:



3. Click **Build All Objects**.

Definitions

1. Under **Component 1>Definitions**, right click and choose variables.
2. Under **Settings** window for **Variables**, enter the following settings:

Name	Expression	Unit	Description
rho	$\rho_0 + \beta \cdot c \cdot (c > 0)$	kg/m ³	Water density

Materials

1. Under **Model Builder>Component 1 (comp 1)**, right click on **Materials** and choose **Add Material from Library**.
2. Select **Water** from **Add Material** window and click **Add to Component**.
3. Again, under **Model Builder>Component 1 (comp 1)**, right click on **Materials** and choose **Blank Material**.
4. Under **Settings** window, label it as **Porous Media** and enter porosity and permeability values as **epsilon** and **kappa** respectively.

Darcy's Law (dl)

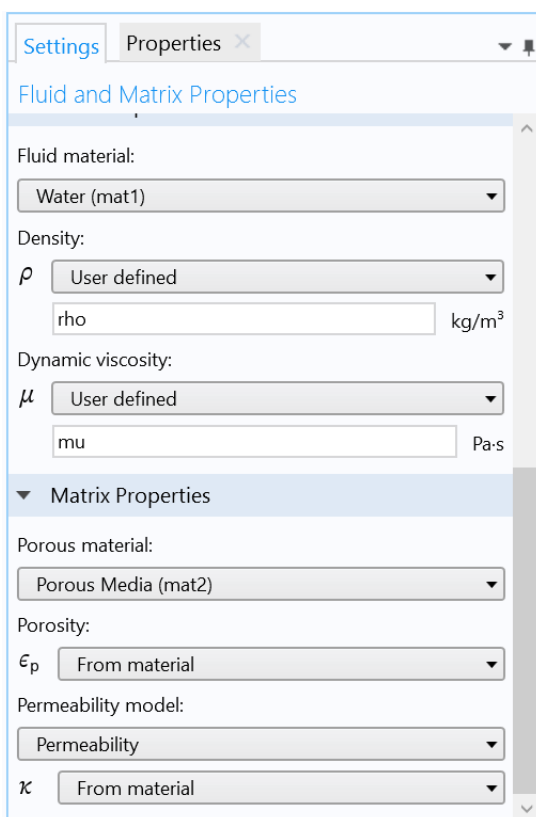
1. Under **Model Builder>Component 1 (comp 1)**, click **Darcy's Law (dl)**.
2. Under **Settings** window for **Darcy's Law**, go to **Gravity Effects** select **Include gravity**.

Gravity 1

1. Under **Model Builder**>**Component 1 (comp 1)**>**Darcy's Law (dl)**, click **Gravity 1**.
2. Under **Settings** window for **Gravity**, go to Specify list and choose **Elevation**.
3. Type **z-L** in the **D** text field.

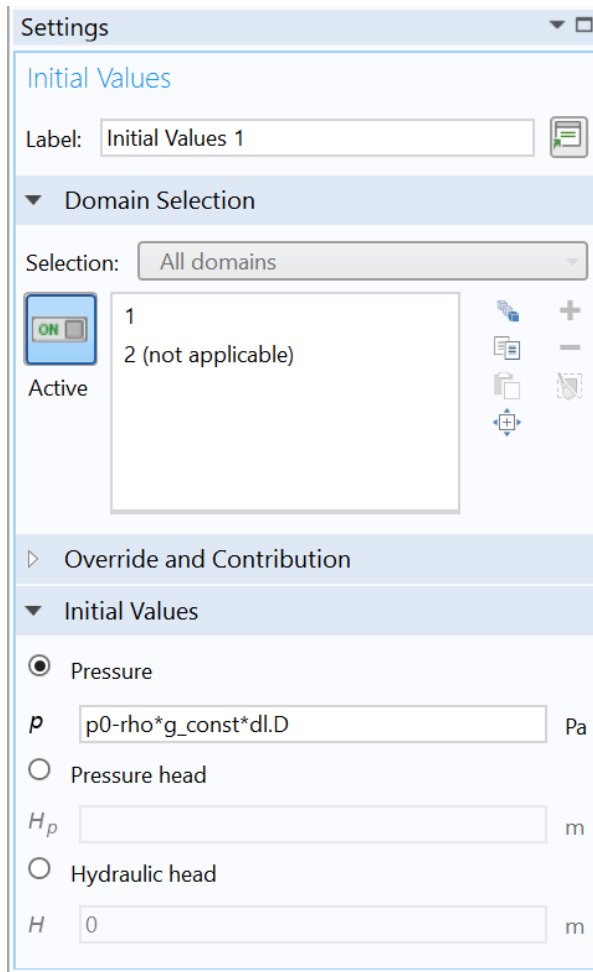
Fluid and Matrix Properties 1

1. Under **Model Builder**>**Component 1 (comp 1)**>**Darcy's Law (dl)**, click **Fluid and Matrix Properties 1**.
2. Under **Settings** window for **Fluid and Matrix Properties**, enter the following settings.



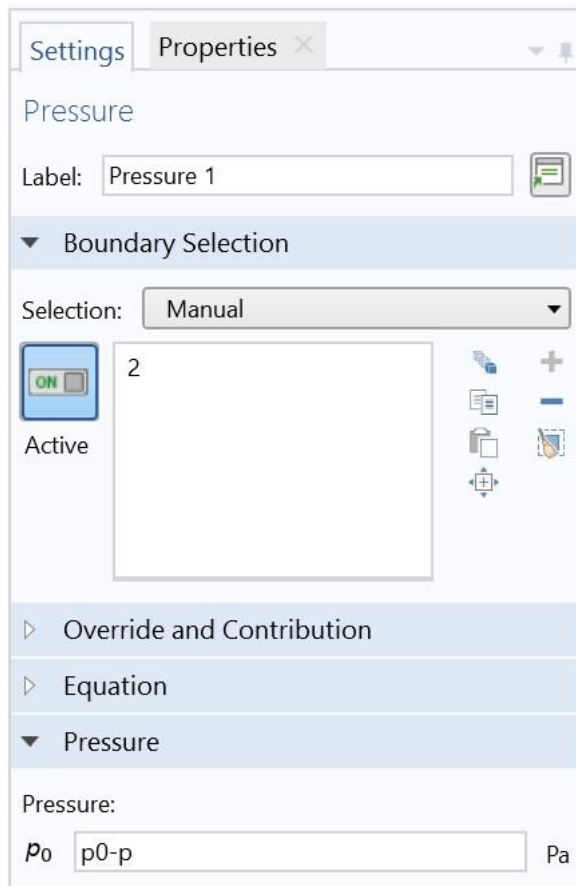
Initial Values 1

1. Under **Model Builder**>**Component 1 (comp 1)**>**Darcy's Law (dl)**, click **Initial Values 1**.
2. Under **Settings** window for **Initial Values**, enter the following settings.



Pressure 1

1. In the **Physics** toolbar, go to **Boundaries>Darcy's law** and click **Pressure**.
2. Under **Pressure 1** in **Model Builder**, enter the following settings.



Transport of Diluted Species (tds)

1. In the **Model Builder** window, under **Component 1**, right click on **Transport of Diluted Species (tds)** and add **Porous Media Transport Properties**.
2. Right click again on **Transport of Diluted Species (tds)** and add **Initial Values**.

These will appear as **Porous Media Transport Properties 1** and **Initial Values 2** respectively.

Transport Properties 1

1. In the **Model Builder** window, go to **Component 1>Transport of Diluted Species (tds)>Transport Properties 1**.
2. Under **Settings>Domain Selection**, choose the domain containing CO₂ gas column.
3. Under **Settings>Convection**, enter the following settings:

Velocity field:

u User defined

0	r	m/s
0	z	

▼ Diffusion

Material:

None

Diffusion coefficient:

D_c User defined

1.6e-5[m²/s] m²/s

Isotropic

No Flux 1

1. In the **Model Builder** window, go to **Component 1>Transport of Diluted Species (tds)>No Flux 1**.
2. Under **Settings** window, go to **Convection** and check **Include**.

Initial Values 1

1. In the **Model Builder** window, go to **Component 1>Transport of Diluted Species (tds)>Initial Values 1**.
2. Under **Settings** window, go to **Initial values**.
3. In concentration, enter c_0 .

Porous Media Transport Properties 1

1. In the **Model Builder** window, go to **Component 1>Transport of Diluted Species (tds)>Porous Media Transport Properties 1**.
2. Under **Settings>Domain Selection**, choose the domain containing porous medium.
3. In the **Settings** window, enter the following settings:

▼ **Matrix Properties**

Porous material:

Porosity:
 ϵ_p

▼ **Convection**

Velocity field:
 \mathbf{u}  

▼ **Diffusion**

$$D_{e,j} = \frac{\epsilon_p}{\tau_{F,j}} D_{F,j}$$

Fluid material:

Fluid diffusion coefficient:
 $D_{F,c}$ m²/s

Effective diffusivity model:

$\tau_{F,c}$ 1

Initial Values 2

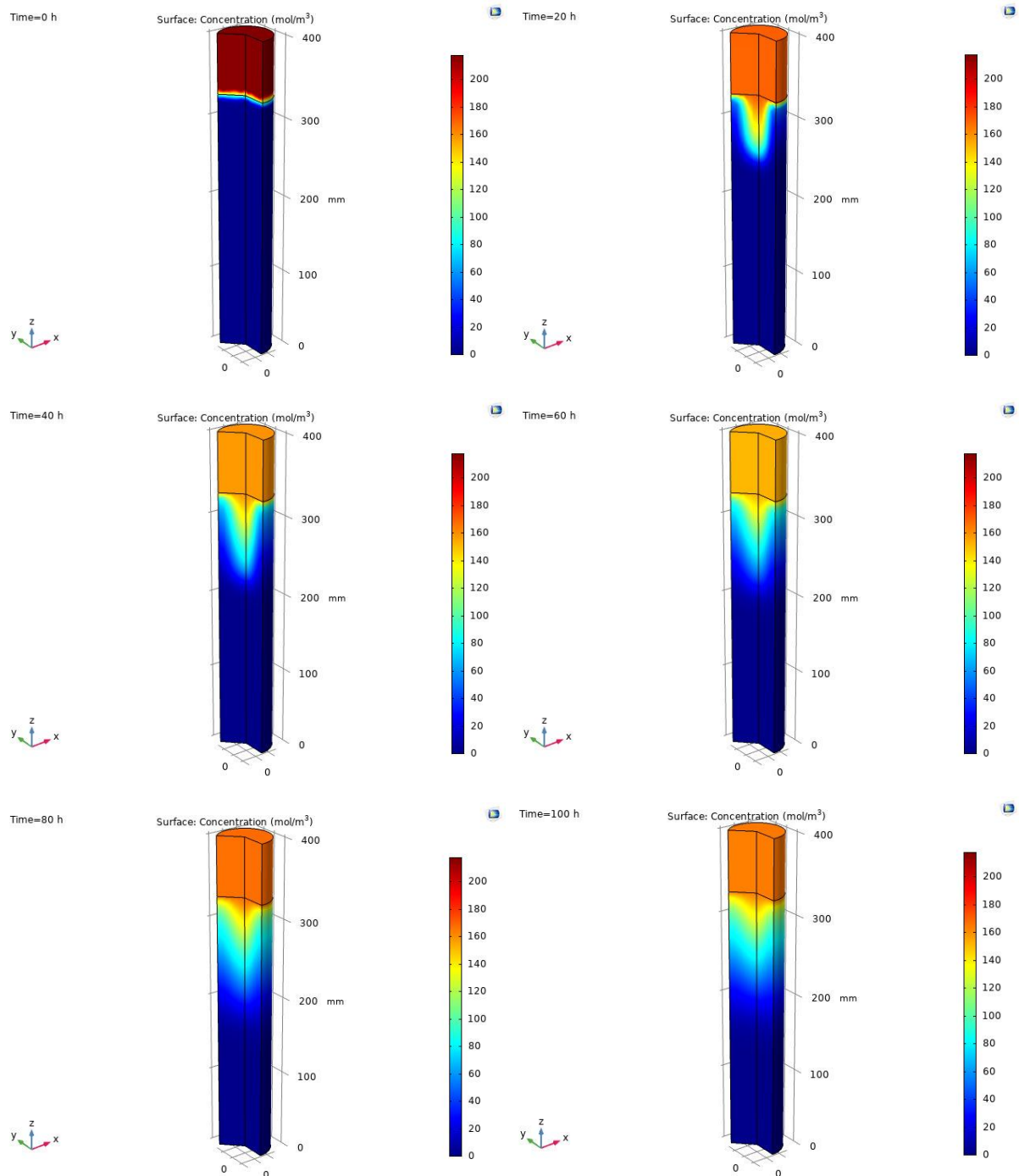
4. In the **Model Builder** window, go to **Component 1>Transport of Diluted Species (tds)>Initial Values 2**.
5. Under **Settings** window, go to **Initial values**.
6. In concentration, enter **c_s**.

Under **Mesh 1** in the **Model Builder** window, choose the choose the desired element size for mesh creation and click **Build All**.

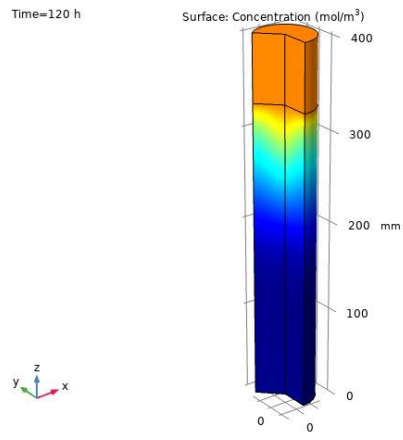
Under **Study 1>Step 1: Time Dependent** in the **Model Builder** window, choose the desired time unit and time range for simulation.

Appendix B

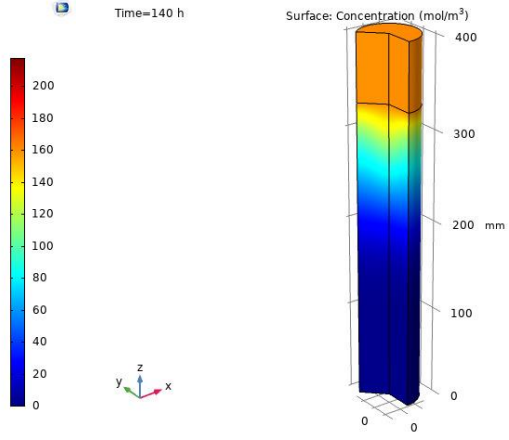
Mixing regime in WSPM of 45% porosity and 23800 mD permeability from $t=0$ to $t=460$ hours obtained from COMSOL simulation:



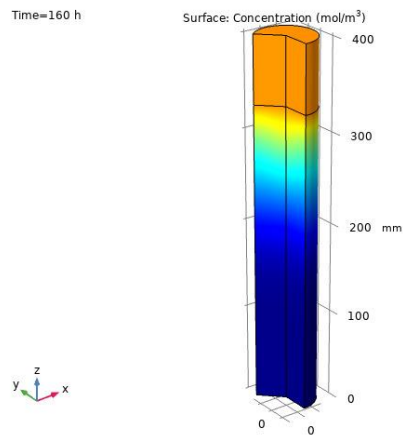
Time=120 h



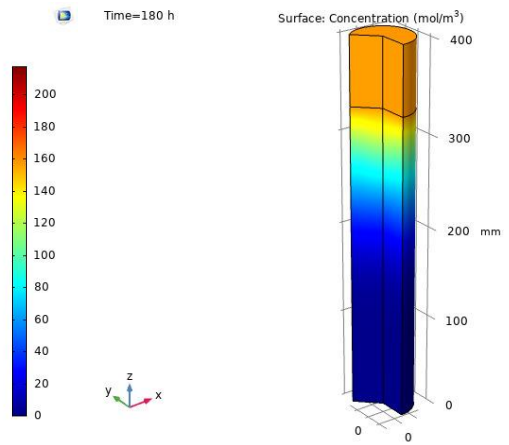
Time=140 h



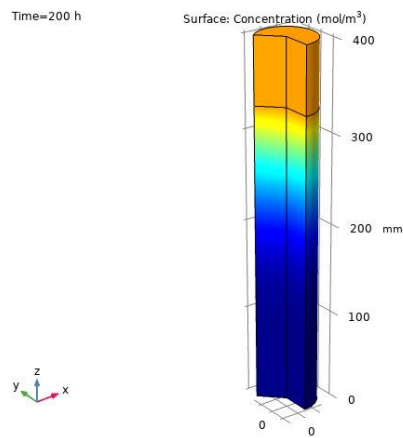
Time=160 h



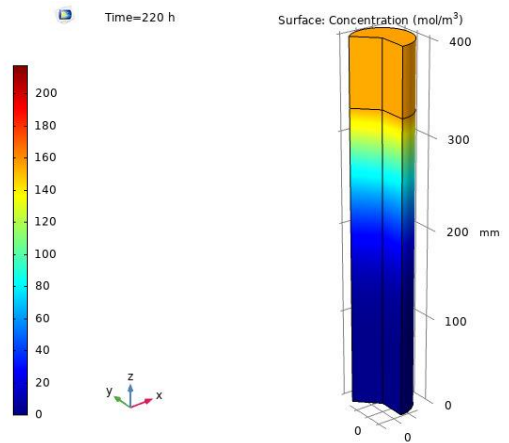
Time=180 h



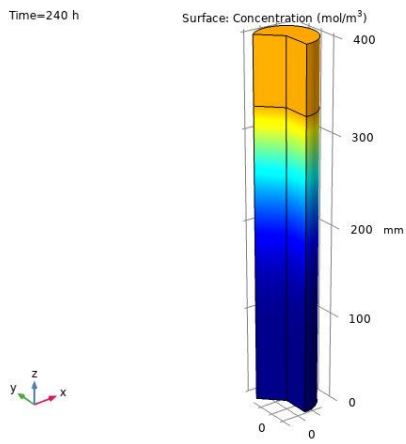
Time=200 h



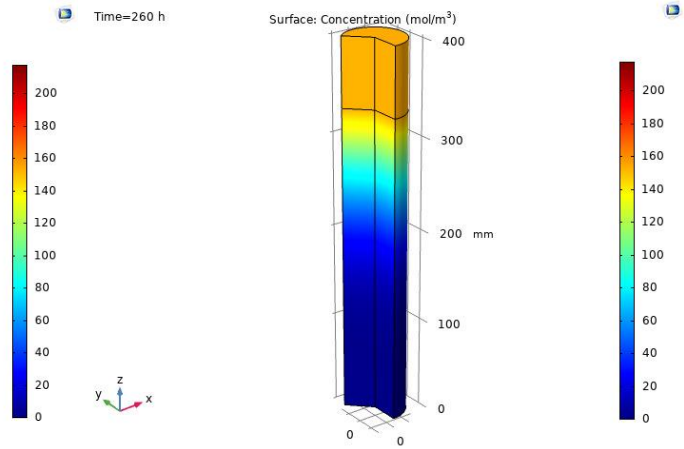
Time=220 h



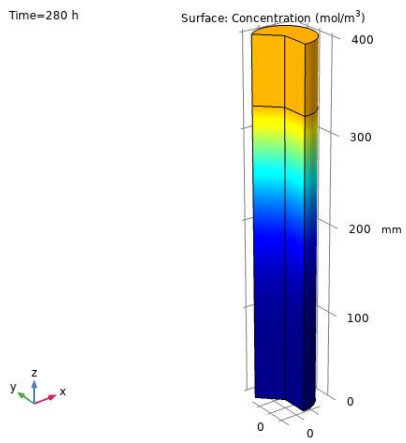
Time=240 h



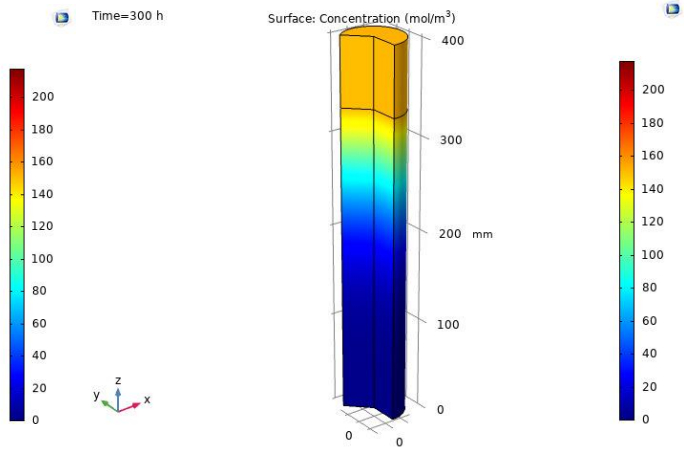
Time=260 h



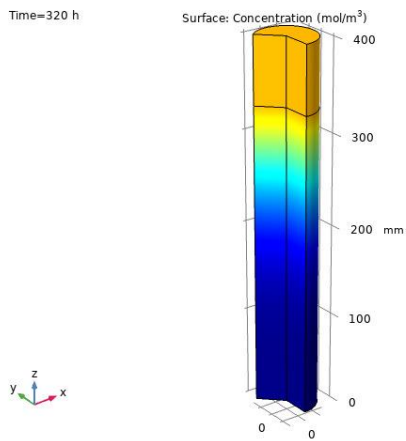
Time=280 h



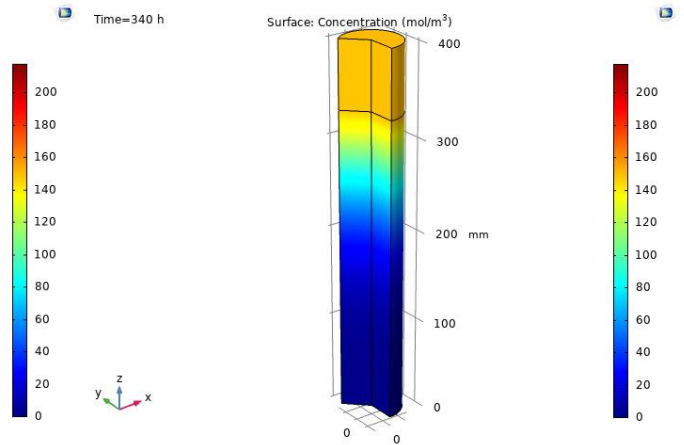
Time=300 h



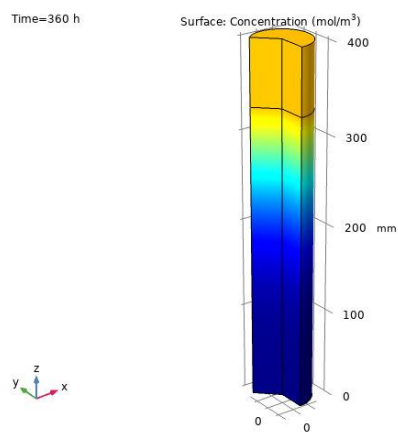
Time=320 h



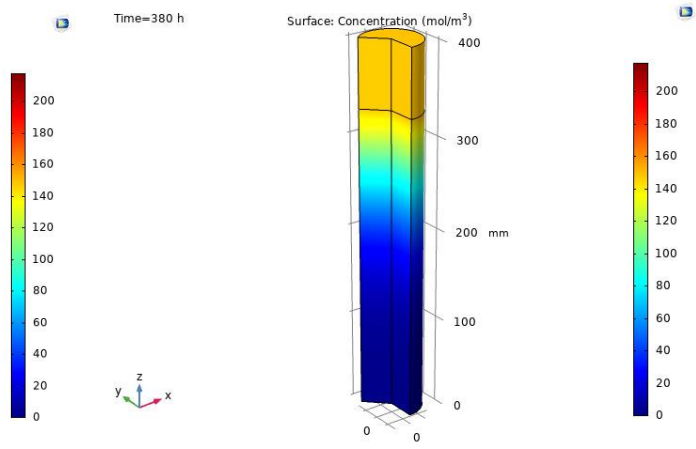
Time=340 h



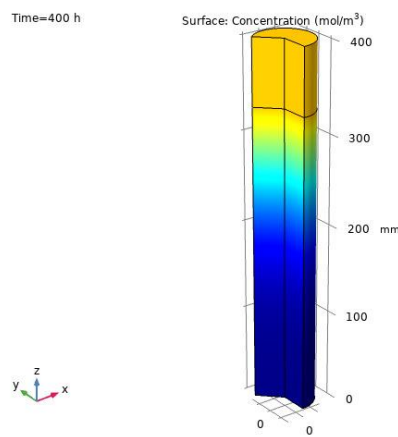
Time=360 h



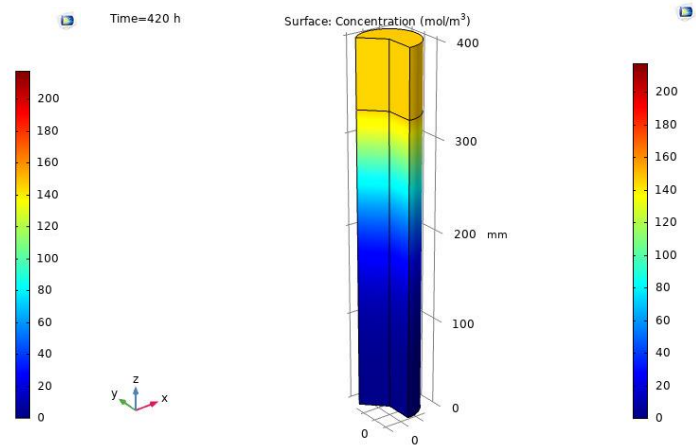
Time=380 h



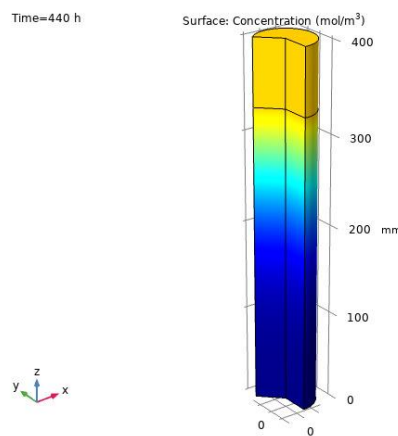
Time=400 h



Time=420 h



Time=440 h



Time=460 h

